Interfacial solar steam generation by wood-based devices to produce drinking water: a review

Roya Mehrkhah, Elaheh K. Goharshadi, Eric Lichtfouse, Ho Seon Ahn, Somchai Wongwises, Wei Yu, Omid Mahian

▶ **To cite this version:**

Roya Mehrkhah, Elaheh K. Goharshadi, Eric Lichtfouse, Ho Seon Ahn, Somchai Wongwises, et al.. Interfacial solar steam generation by wood-based devices to produce drinking water: a review. Environmental Chemistry Letters, 2023, 21 (1), pp.285-318. 10.1007/s10311-022-01501-1 . hal-03776534

HAL Id: hal-03776534
https://hal.science/hal-03776534

Submitted on 13 Sep 2022

HAL is a multi-disciplinary open access archive for the deposit and dissemination of scientific research documents, whether they are published or not. The documents may come from teaching and research institutions in France or abroad, or from public or private research centers.

L'archive ouverte pluridisciplinaire **HAL**, est destinée au dépôt et à la diffusion de documents scientifiques de niveau recherche, publiés ou non, émanant des établissements d'enseignement et de recherche français ou étrangers, des laboratoires publics ou privés.

Environmental Chemistry Letters
https://doi.org/10.1007/s10311-022-01501-1

REVIEW

Interfacial solar steam generation by wood-based devices to produce drinking water: a review

Roya Mehrkhah[1] · Elaheh K. Goharshadi[1,2,3] · Eric Lichtfouse[4,5] · Ho Seon Ahn[6,7] · Somchai Wongwises[8,12] · Wei Yu[9,10] · Omid Mahian[11]

Abstract

Freshwater supply is declining in the context of climate change, pollution, and soil salinization, calling for sustainable meth-ods to produce drinking water. For instance, salt water can be converted into pure water by steam generation. Interfacial solar steam generation involves photoabsorbers consisting of a photothermal material with broad solar absorption and a porous substrate with a thermal insulating character. Nonetheless, scaling up of classical devices for interfacial solar steam genera-tion is actually limited by cost, biofilm formation, salt fouling, complicated fabrication processes, and toxicity. Alternatively, wood-based devices are cheap, biodegradable, abundant, and display high fluxes of evaporation compared with other non-biodegradable photoabsorbers. Here we review the design and applications of wood-based solar steam generation devices, with focus on wood structure and properties, different types of devices, and factors controlling the evaporative performance.

Keywords Freshwater · Nanomaterials · Biodegradable · Photoabsorber · Wood-based solar steam generation devices · Low cost

Introduction

Freshwater availability is essential for the survival of the living organisms (Deng et al. 2017; Villaseñor and Ríos, 2018; Wang et al. 2021a, b, c, d). Today, 1.1 billion people suffer from water scarcity worldwide, especially in develop-ing countries and remote areas (Ercin and Hoekstra, 2014; Gong et al. 2021; Hassan and Yousef, 2021; Mekonnen and Hoekstra, 2016; Mu et al. 2021; Sheng et al. 2020; Sun et al. 2020a, b; Xu et al. 2021). About 70% of water sources on

✉ Roya Mehrkhah
mehrkhahroya@gmail.com

✉ Ho Seon Ahn
hsahn@inu.ac.kr

✉ Omid Mahian
omid.mahian@xjtu.edu.cn

Eric Lichtfouse
eric.lichtfouse@gmail.com

[1] Department of Chemistry, Faculty of Science, Ferdowsi University of Mashhad, Mashhad 9177948974, Iran

[2] Nano Research Center, Ferdowsi University of Mashhad, Mashhad 9177948974, Iran

[3] Center for Nanotechnology in Renewable Energies, Ferdowsi University of Mashhad, Mashhad 9177948974, Iran

[4] State Key Laboratory of Multiphase Flow in Power Engineering, Xi'an Jiaotong University, Xi'an 710049, China

[5] Aix Marseille Univ, CNRS, IRD, INRAE, CEREGE, Aix-en-Provence, France

[6] Department of Mechanical Engineering, Incheon National University, Incheon, South Korea

[7] Nuclear Safety Research Institute, Incheon National University, Incheon, South Korea

[8] Fluid Mechanics, Thermal Engineering and Multiphase Flow Research Laboratory (FUTURE), Department of Mechanical Engineering, Faculty of Engineering, King Mongkut's University of Technology Thonburi (KMUTT), Bangmod, Bangkok 10140, Thailand

[9] School of Energy and Materials, Shanghai Key Laboratory of Engineering Materials Application and Evaluation, Shanghai Polytechnic University, Shanghai 201209, China

[10] Shanghai Engineering Research Center of Advanced Thermal Functional Materials, Shanghai 201209, China

[11] School of Chemical Engineering and Technology, Xi'an Jiaotong University, Xi'an 710049, Shaanxi, China

[12] National Science and Technology Development Agency (NSTDA), Pathum Thani 12120, Thailand

the earth are seawater that cannot be used directly (Li et al. 2018a, b, c, d; Ramanathan et al. 2018). Therefore, it is vital to find a suitable and efficient desalination method for producing drinking water. Solar steam generation is a promising method for desalinating saline water (Arunkumar et al. 2019; Xu et al. 2020). Solar steam generation methods are classified into two categories: volumetric and interfacial.

Volumetric solar steam generation devices composed of nanofluids or suspending nanomaterials in base fluids suffer from several obstacles such as instability of the nanofluids, high production costs, and exposure to radiation, conduction, and convection heat loss due to inevitable heating of the bulk liquid (Amjad et al. 2018; Babita et al. 2016; Bakthavatchalam et al. 2020; Chen et al. 2018; Colangelo et al. 2016; Gao et al. 2019a, b; Ghafurian et al. 2020a; Goharshadi et al. 2013a, b; Hajatzadeh Pordanjani et al. 2019; Li et al. 2019b, c, a; Liu et al. 2018a, b, c, d; Liu and Xuan, 2017; Mahian et al. 2019; Mehrkhah et al. 2022; Pilch-wr et al. 2021; Sheikhpour et al. 2020; Struchalin et al. 2021; Wang et al. 2016a, b; Zareei et al. 2019; Zeiny et al. 2018). The interfacial solar steam generation devices consist of a double-layer photoabsorber at the seawater's surface (Amjad et al. 2018; Colangelo et al. 2016; Deng et al. 2017; Gao et al. 2019a, b; Struchalin et al. 2021). The top layer is a photothermal material that absorbs the sunlight and converts it into thermal energy efficiently. The bottom layer, aptly called the substrate, is a thermal insulator that continuously pumps water to the top layer (Wang et al. 2016a, b).

In interfacial solar steam generation devices, the photothermal conversion is confined at the water–air interface so that only water at the surface is heated (Gao et al. 2019a, b; Peng et al. 2021; Zhao et al. 2020). In addition, the photoabsorber's surface temperature remains low, resulting in reduction of radiation and convection heat loss at the photoabsorber's surface (Liu et al. 2017a, b, c; Ren et al. 2017; Wang et al. 2017a; Zhang et al. 2017; Zhou et al. 2016). Hence, the interfacial solar steam generation is an environmentally friendly, low-energy consuming, and efficient technique compared to the volumetric solar steam generation method that can be used for desalinating seawater, sterilization, electricity generation, wastewater treatment, and photothermal conversion (Darling, 2018; Ghafurian et al. 2021; Irani et al. 2021; Jin et al. 2016; Li et al. 2018b, 2017a; Li et al. 2021a, b, c, d; Lin et al. 2019; Liu et al. 2017a, b, c; Ni et al. 2016; Tao et al. 2018; Wang et al. 2017b; Wang et al. 2021a, b, c, d; Wang et al. 2021a, b, c, d, 2016a, b; Zehtabiyan-Rezaie et al. 2021; Zhang et al. 2018a, b; Zhang et al. 2020a, b, c; Zhou et al. 2016; Zhu et al. 2019a, b, c, 2018a, b; Zielinski et al. 2016).

To date, different types of photothermal nanomaterials such as noble metal nanoparticles, including Ag and Pd, semiconductor nanoparticles such as VO_2 (insulating monoclinic phase), carbonaceous nanomaterials such as graphene and reduce graphene oxide composite aerogels, polymers such as polyethylene foam, and biomass carbon nanomaterials such as porous carbonized lotus seedpods and surface-carbonized desugaring stems of sugarcane have been used in interfacial solar steam generation devices (Awad et al. 2018; Aziznezhad et al. 2020; Cao et al. 2021; Chen et al. 2021; Ding et al. 2021; Fang et al. 2018, 2017; Ghafurian et al. 2020c; Hu et al. 2017; Huang et al. 2017; Ibrahim et al. 2020; Jilani et al. 2018; Li et al. 2021a, b, c, d; Liu et al. 2021; Liu et al. 2019a, b, c; Liu et al. 2018a, b, c, d; Noureen et al. 2021; Qin et al. 2021; Wang et al. 2017a, b, c; Wei et al. 2021; Xing et al. 2019; Zhang et al. 2021; Zhu et al. 2018a, b).

Several materials with hydrophilic, porous, and thermal insulation properties have been used as a substrate, such as carbon foam, gauze, polystyrene foam, and polymeric compounds in interfacial solar steam generation devices (Chen et al. 2019a, b; Elsheikh et al. 2019; Liu et al. 2019a, b, c; Liu et al. 2015; Qiu et al. 2019; Wang et al. 2021a, b, c, d;; Wu et al. 2019a, b, c; Xiao et al. 2021). However, high cost, complex manufacturing processes, and toxicity of such substrates limit their practical applications (Lee et al. 2020). For example, using organic substrates such as polystyrene foam is not environmentally friendly and can increase plastic pollution (Fang et al. 2018). In contrast, natural materials such as wood have also been used as a low-cost, abundant, green, and sustainable substrates (Fu et al. 2018a, b; Huang et al. 2019; Jia et al. 2017b; Liu et al. 2018a, b, c, d; Wu et al. 2019a, b, c; Xu et al. 2017; Xue et al. 2017; Zhang et al. 2020a, b, c; Zhang et al. 2018a, b; Zou et al. 2021). Wood coated with suitable photothermal nanomaterials can function as a highly efficient interfacial solar steam generation device. Here, we review the design and applications of wood-based solar steam generation devices with focus on wood structure, types, and stability of wood-based devices, and factors influencing on the evaporative performance.

Molecular structure of wood

The study of wood structure is highly important for human civilization development and reducing the use of nonrenewable resources (Jia et al. 2017b). Wood-based substrates in interfacial solar steam generation have several advantages, including excellent hydrophilicity, abundant natural microchannels, superior mechanical stability, light-harvesting properties, light structure, and strong mechanical properties (Fu et al. 2018a, b; Xue et al. 2017). Wood is a good thermal insulator with low distortion and efficient water transfer properties in interfacial solar steam generation (Chen et al. 2017a; Xue et al. 2017). Wood's low thermal conductivity is important for heat localization. In addition, natural wood is cost-effective and has high availability, a wide surface area, and good buoyancy (Chen et al. 2017a; Liu et al. 2018a, b, c, d). In particular, wood's rough surface has a large surface

area, resulting in high-light absorption. Several aligned microchannels of wood can redissolve water-soluble salts in the water and are useful for water transfer (Chen et al. 2017a, b, c; He et al. 2019a, b; Tao et al. 2019).

Wood is composed of lignin, cellulose, and hemicellulose (Jia et al. 2017b; Ren et al. 2021). Cellulose is made of units of β-D-glucopyranose and hemicellulose (a group of polysaccharides consisting of mannans, xyloglucans, xylans, β-glucans, and glucomannans) and strengthens the cell wall via interactions with lignin (Akhlamadi and Goharshadi, 2021; Jia et al. 2017b). Lignin, which is a phenolic polymer consisting of the polymerization of monolignols, including sinapyl alcohol, p-coumaryl alcohol, and coniferyl alcohol, maintains stem strength and cell structure integrity (Jia et al. 2017b). Hemicellulose and cellulose have numerous highly hydrophilic groups including hydroxyl, which result in excellent cell wall hydrophilicity and wood structure. Figure 1 shows an image of the molecular structures of wood. Due to changes in the hierarchical structures, several types of wood species have different porosities, thermal conductivities, and mechanical properties, which are suitable for various applications (Jia et al. 2017b).

Microchannels

Water transfer in the tree, which is critical to the photosynthesis process, is achieved through the rich porous structure, vertical microchannels, and pits. Changes in wood microstructures lead to significantly different functions in interfacial solar steam generation (Ghafurian et al. 2020c). The presence of microchannels in wood and their ability to quickly transfer water allow wood to be used in several fields, including transparent materials, water purification, energy storage, electronic devices, building materials, and composites (Carrillo et al. 2016; Chen et al. 2017b; Chen et al. 2017a, b, c; Jia et al. 2017a; Jung et al. 2015; Li et al. 2016a, b; Xu et al. 2016; Zhu et al. 2016a; Zhu et al. 2017b). Figure 2 presents the cross-section scanning electron microscopy images of microchannels. As shown, fiber tracheids and vessels with different diameters act as pathways for water transfer and the pits provide connections between the tracheids and vessels. The capillary action of wood and its porous and hydrophilic structure play an important role in water transfer from roots to tree leaves (Kuang et al. 2019b; Zhong et al. 2019).

Hardwoods and softwoods

According to microstructures, physical structure, and compositions, wood can be divided into hardwood with tracheids and vessels and softwood with only tracheids (Gibson, 2012). Three types of cells of the tracheids, vessels, and parenchyma make up hardwood. The tracheids with a smaller diameter support the wood structure, and the vessels with a larger diameter help water transfer. Softwood formed by the tracheids and parenchyma transfers water through the pits. The tracheids

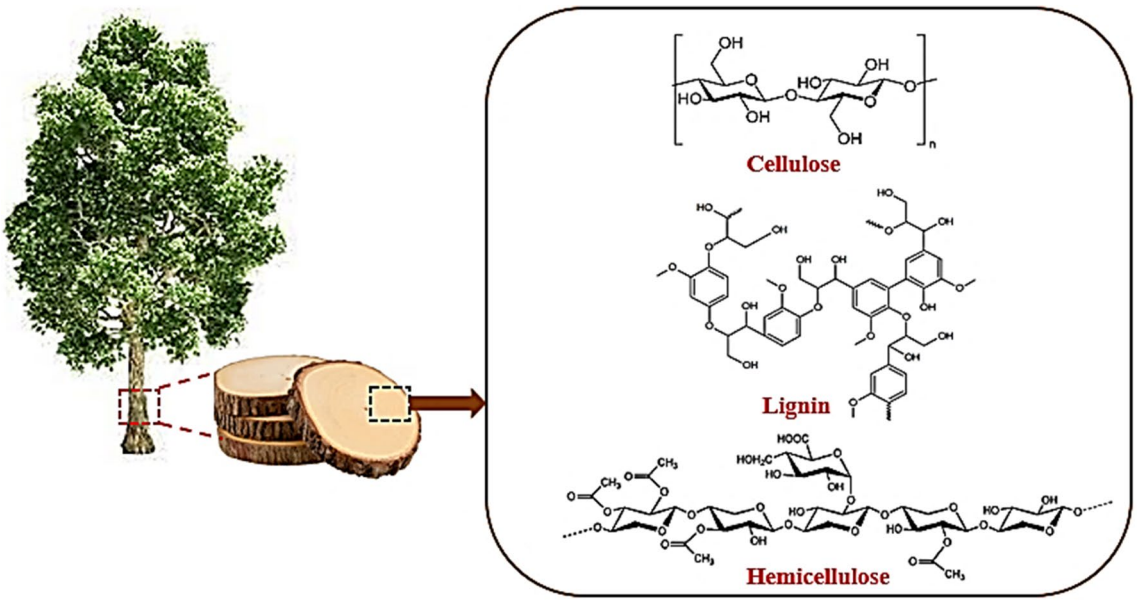

Fig. 1 Molecular structure of cellulose, hemicellulose, and lignin of wood. Cellulose is made of units of β-D-glucopyranose and hemicellulose. Lignin consists of the polymerization of monolignols, including sinapyl alcohol, p-coumaryl alcohol, and coniferyl alcohol. Interaction between lignin and cellulose leads to the cell wall strength. Lignin also maintains stem strength and cell structure integrity. Hemicellulose is a composed of polymerization of 100–200 glucose units. Hemicellulose structure containing many branches, including acetyl groups, is more complex than cellulose

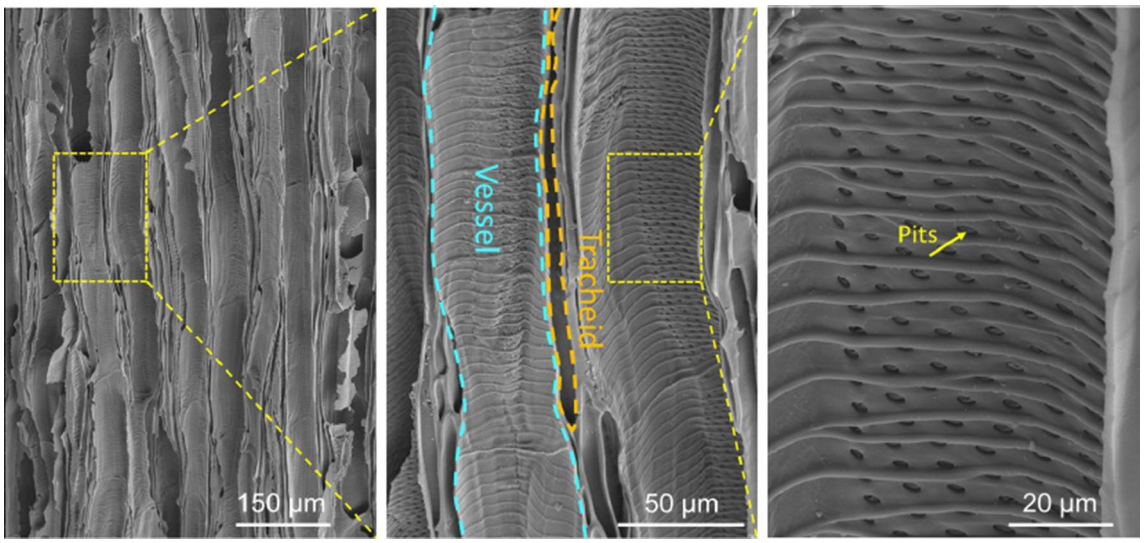

Fig. 2 Cross-sectional scanning electron microscopy images illustrating microchannel structure of wood and pits on the cell walls. Water supply plays an essential role in the solar steam-generation process, and capillarity is the primary driving factor for water transport through the wood channels. Hence, the capillary effect of wood is studied by scanning electron microscopy to determine its ability to supply water. The cylindrical wood microchannels, including large-sized vessels and small-sized tracheids, are responsible for the water transport from the bulk to the photothermally active layer of the photoabsorber. The pits play a vital role in horizontal water transfer to the photothermal layer. The pits function as pathways for fast salt exchange between channels with interconnecting the vessels with the tracheids. Reproduced with permission of Wiley from Kuang et al. (2019b)

connected via the pits provide a mechanical support and transfer fluids throughout wood. Hardwoods come from trees with broad leaves whose seeds are in fruits or pods.

Common hardwoods include balsa, bass, cocobolo, elm, locust, maple, oak, olive, padauk, and poplar. Softwoods come from evergreen trees that have needles and cones throughout the year. Common softwoods include cedar, pine, and yew. Hardwoods have a more complex structure compared to softwoods and therefore grow less rapidly. Despite structural differences, hardwood and softwood have similar microchannels and interconnected pore networks that enable water transport in interfacial solar steam generation applications (Jia et al. 2017b). The vessels' presence in hardwood constitutes a significant difference between hard and softwoods. Hard and softwoods consist of cellulose nanofibers, which make the natural wood very strong (Jia et al. 2017b).

Physicochemical properties of wood

Thermal conductivity

Natural wood has a very low thermal conductivity, of about 0.45 W m^{-1} K^{-1} for wet wood, and wood's poor heat transfer property helps to localize the heat in the evaporation layer. This is because it prevents heat transfer into the wood matrix, making wood as a thermal insulation substrate for efficient interfacial solar steam generation (Kim et al. 2018; Wang et al. 2019a, b, c; Zhu et al. 2018a, b). Wood has different thermal conductivities in several directions of wood due to its anisotropic structure. Heat conduction in the axial direction is greater than it is in the transverse direction due to the channels' natural alignment and wood's high porosity (Li et al. 2018a, b, c, d).

Wood can be cut vertically in the direction of tree growth (Fig. 3a) and horizontally perpendicular to the direction of tree growth (Fig. 3b). The thermal conductivity of wood also depends on its density so that as wood density rises, the thermal conductivity increases for both vertically and horizontally cut wood (Jia et al. 2017b; He Liu et al. 2018a, b, c, d). The different directions of wood convey the anisotropic mechanical properties. Vertically cut woods show higher mechanical strength compared to horizontally cut woods. The thermal conductivities of poplar, pine, and cocobolo vertically and horizontally cut woods were compared, and the results revealed that the thermal conductivity of horizontally cut woods (0.27, 0.32, and 0.34 W m^{-1} K^{-1} for poplar, pine, and cocobolo wood, respectively) is higher than that of vertically cut woods (0.12, 0.14, and 0.21 W m^{-1} K^{-1}, respectively) (Vay et al. 2015).

Density and porosity

Since the structure of several kinds of wood differs resulting in differences in their properties, such as density and porosity, which can change the wood performance in interfacial solar steam generation applications (Jia et al. 2017b),

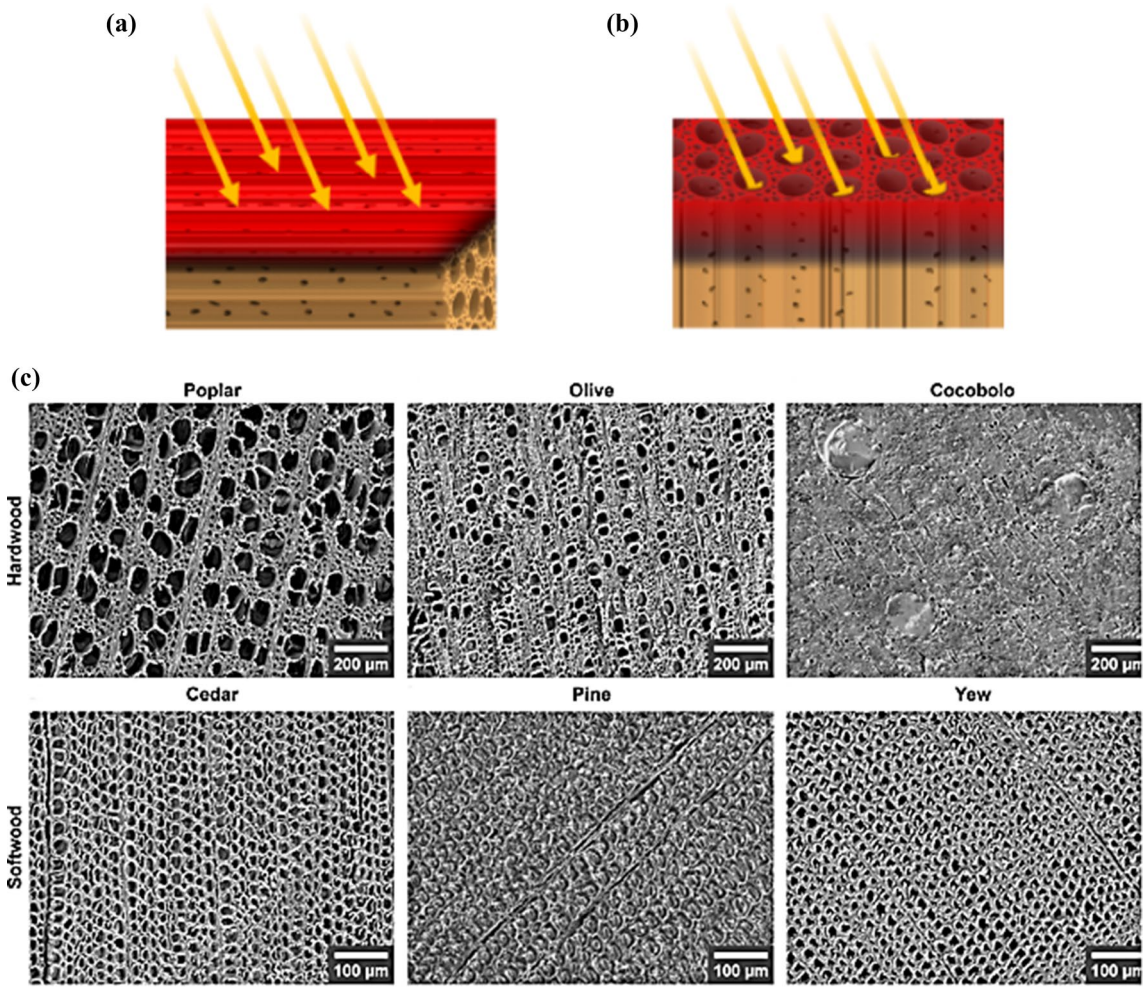

Fig. 3 Heat localization on the surface of **a** vertically cut wood and **b** horizontally cut wood. An anisotropic thermal conductivity is observed in several directions of wood. The wood microchannels will be able to block the heat, contributing to greater heat localization. Compared to the horizontally cut wood, the better heat localization is observed in the vertically cut wood that is so crucial for high steam evaporation efficiency. Reproduced with permission.(Liu et al. 2018a, b, c, d) Copyright 2018, Wiley. **c** Scanning electron microscopy images of porous structure of poplar, olive, and cocobolo hardwoods and cedar, pine, and yew softwoods. Several wood types have different porous structures. As shown in top view scanning electron microscopy images, an obvious difference is exhibited in lumen diameter of the vessels and tracheids in several hardwoods due to different pore diameter distributions. Softwoods have homogeneous pores in comparison with hardwoods. The different pore size results in different density and porosity. Reproduced with permission of Joule from Jia et al. (2017b)

the density may vary from 175 for the balsa wood to more than 1000 kg m^{-3} for some types of sandal wood. The bulk density of natural wood, ρ, is calculated using the following equation (Wang et al. 2019a, b, c):

$$\rho = \frac{m}{V} \tag{1}$$

where m is the mass and V is the volume of wood.

Porosity, $\emptyset$, is an effective property of wood that affects the interfacial solar steam generation efficiency (Y. Wang et al. 2016a, b). Different types of wood have different porosities. The porosity is calculated using Eq. 2 (Ghafurian et al. 2020b):

$$\emptyset = \frac{m - m_O}{V\rho_w} \tag{2}$$

where m_o and m are the mass of wood before and after water absorption, respectively. ρ_w is the density of water. Obviously, a decrease in the porosity results in an increase in density (Ghafurian et al. 2020b).

Figure 3c illustrates top surface scanning electron microscopy images of poplar, olive, and cocobolo hardwoods, and cedar, pine, and yew softwoods. As this figure shows, differences exist in the diameter of vessels and tracheids of hardwoods. Various pore sizes lead to different porosities and densities so that hardwoods with high porosity have low density

and high heat insulation properties. On the contrary, cedar, pine, and yew softwoods have homogeneous pores. An obvious difference exits in the density of hardwoods. For example, the density of poplar wood is twice as low as cocobolo wood, resulting in a high porosity of 66%. Low difference in the density and porosity of softwoods shows their structures that are more uniform (Jia et al. 2017b).

Lignin is removed for accelerating the water transfer to the surface, decreasing density, and increasing wood porosity (Donaldson et al. 2018; Zhu et al. 2016b). Table 1 shows the porosity and density of several wood types before and after delignification. As Table 1 shows, an increase in porosity and a decrease in density are observed after the delignification process of several wood types. Among them, poplar wood has the least density and most porosity.

Capillary action

Due to the water molecules' cohesive forces and wood's capillary action, water is transferred from the bulk into the wood surface (Ghafurian et al. 2020c). A trade-off between the rate of water transfer to the evaporative surface and the rate of the evaporation causes the solar steam to be continuously generated and the photoabsorber's surface remains wet during interfacial solar steam generation (Ghafurian et al. 2020c). All following equations have been utilized for reaching an equation describing the effect of wood texture on the speed of water transfer from the bulk to the evaporative surface. The flow rate through the wood's permeable medium caused by the arrays of microchannels is calculated according to Darcy's law (Jia et al. 2017b):

$$Q = -\frac{k\Delta P}{\mu\beta} \tag{3}$$

Table 1 Density and porosity of several wood types before and after delignification. Reproduced with permission of Elsevier from Ghafurian et al. (2020c)

Sample	ρ(g cm^{-3})		∅(%)	
	Before	After	Before	After
Poplar	524.7	461.3	66.6	79.0
Grape	549.7	489.7	64.5	75.5
Pine	596.1	536.5	63.8	73.9
Plantain	618.1	559.2	63.8	73.9
Maple	619.6	565.7	59.9	68.4
Walnut	632.4	585.8	58.9	66.2
Yew	679.3	634.4	56.0	62.6
Barberry	690.0	652.0	55.5	61.0
Service	696.9	660.6	55.2	60.4
Beech	703.5	675.3	54.7	58.8
Ulmus glabra	811.9	790.7	47.7	50.3
Jujube	942.3	914.0	39.2	42.2

where Q stands for the flow rate per unit area (m s^{-1}), k is wood permeability (m^2), μ is the viscosity of the fluid (Pa.s), and β is the wood thickness (m). ΔP is the difference of the pressure between two ends of the microchannels (Pa) (Jia et al. 2017b). As this equation shows, an increase in the permeability of wood leads to the increase of flow rate in the microchannels. The Carman–Kozeny equation is used for the normalization of permeability (Lee et al. 2020):

$$\frac{k}{d_h^2} = \frac{\emptyset}{16K} \tag{4}$$

where k is wood permeability. ∅ stands for the porosity. d_h denotes the hydraulic diameter of the membrane. K is the Kozeny constant. Considering the Kozeny constant increases at a high porosity (> 80%), the normalized permeability, $K\,d_h^{-2}$, decreases in very porous media (with > 80% porosity) resulting in the increase of the flow rate of water (Yang et al. 2010).

Equation 3 specifies the effect of the wood texture on water flow rate, where porosity, pores diameter, and the tortuosity of the wood vessels play important roles (Ghafurian et al. 2020b). The relationship between the flow rate and wood texture is achieved according to Eqs. 5–10:

The relationship between permeability, k, porosity, ∅, and the diameter of the microchannel, d, is shown by Eq. 5:

$$k = \frac{\emptyset d^2}{32\tau} \tag{5}$$

where τ stands for the microchannels' tortuosity.

The pressure caused by the surface tension and hydrostatic pressure is calculated by Eqs. 6 and 7, respectively (Jia et al. 2017b; Zhou et al. 2019):

$$\Delta P = \frac{4\sigma cos\theta}{r} \tag{6}$$

where σ is surface tension of the air–liquid. θ denotes the contact angle. r stands for the radius of the pore.

$$P = \rho g\beta \tag{7}$$

where g is the gravity acceleration. ρ stands for the bulk density of natural wood. β is the wood thickness.

The pressure difference, ΔP, that the capillarity causes is calculated by Eq. 8:

$$\Delta P = \frac{4\sigma cos\theta}{d} - \rho g\beta \tag{8}$$

where d is diameter of the microchannel. σ stands for surface tension of the air–liquid. At $\theta = 0$ and using Eqs. 5 and 8, Eq. 3 can be written as follows:

$$Q = \frac{\emptyset d^2}{32\mu\tau}\left(\frac{4\sigma}{d\beta} - \rho g\right) \tag{9}$$

where Q stands for the flow rate per unit area. μ is the viscosity of the fluid. $\emptyset$ stands for the porosity. σ is surface tension of the air–liquid. As $\sigma = 0.072$ N m^{-1}, $\rho = 1000$ kg m^{-3}, and $g = 9.8$ m s^{-2}, $\frac{4\sigma}{dT} >> \rho g$ is obtained, and hence, the flow rate (Eq. 3) is rewritten as (Jia et al. 2017b):

$$Q = \frac{\emptyset d}{4\mu\tau}\frac{\sigma}{\beta} \tag{10}$$

Equation 10 shows the relationship between the flow rate to the evaporative surface and wood texture, including porosity, pores diameter, the microchannels tortuosity, and thickness. As this equation shows, there is an inverse relationship between wood thickness and the flow rate, so that with increasing the microchannels' length, the amount of water transferred to the evaporative surface reduces. On the other hand, according to Eq. 10, with increasing porosity and diameter of wood pores, the flow rate increases showing each of these parameters is crucial to achieve a high evaporation efficiency in interfacial solar steam generation.

Wood-based solar steam generation devices

Wood-based solar steam generation devices play an important role in reducing the freshwater crisis due to excellent light absorption and water transfer capabilities as well as heat loss prevention (He et al. 2019a, b). Several efforts have been performed to improve the interfacial solar steam generation performance of wood-based devices through optimizing photothermal materials and wood substrate. Wood-based solar steam generation devices in which the wood substrate is treated are named as refined wood-based solar steam generation devices and other photoabsorbers in which wood remains unchanged are named as unrefined wood-based solar steam generation devices. There are several methods for wood surface treatment, including carbonization, flame treatment, delignification process, laser treatment, chemical preparation of flexible wood and wood aerogel, and channel-array design to obtain a wood-based photoabsorber with maximum light-harvesting capabilities (Chen et al. 2017a; Ghafurian et al. 2020b; He et al. 2019a, b; Kim et al. 2018; Kuang et al. 2019b; Liu et al. 2019a, b, c; Xue et al. 2017; Qian Zhang et al. 2020a, b, c). In addition, both vertically and horizontally cut woods can be used in wood-based devices to produce solar steam.

Refined wood-based solar steam generation devices

Several wood-based materials made from treated wood have been used as a substrate for refined wood-based solar steam generation devices. Jia et al. used several wood-based solar steam generation devices consisting of carbonized hard and softwoods, including poplar, pine, and cocobolo (Jia et al. 2017b). They found there was a large difference in interfacial solar steam generation efficiency depending on the kind of wood. They obtained evaporation efficiencies of 86.7, 76.3, and 46.8% under 10 sun for poplar, pine, and cocobolo wood-based solar steam generation devices, respectively. The poplar wood with 66% porosity had the highest efficiency.

Carbonized mesoporous wood with long-term stability and an antifouling property was used to absorb 99% of solar energy and produce efficient interfacial solar steam generation. The carbonized mesoporous wood presented 87% efficiency under 10 sun. However, due to its low flexibility, this photoabsorber cannot be used in large-scale applications (Zhu et al. 2017a). Guobin et al. refined the wood surface with a flame and used it as a photoabsorber. The flame-refined wood absorbed a wide range of solar energy and had open microchannels to transfer water to the evaporative surface. The photoabsorber achieved 72% evaporation efficiency under 1 sun (Xue et al. 2017). A flexible wood prepared using a chemical treatment and coated with carbon nanotubes could achieve 81% efficiency under 10 sun due to excellent light absorption, low thermal conductivity, and hierarchical microchannels (Chen et al. 2017a).

Zhao et al. used carbonized wood as a wood-based photoabsorber and obtained 91.3% efficiency under 1 sun (Liu et al. 2018a, b, c, d). A photoabsorber consisting of titanium nitride and carbonized wood was used for interfacial solar steam generation and could obtain 92.5% evaporation efficiency under 1 sun (Guo and Yang, 2019). Yuming et al. used delignified wood decorated with carbon nanotubes. They found that the interfacial solar steam generation efficiency of delignified wood coated with carbon nanotubes improved by 20% with respect to natural wood coated with carbon nanotubes under ambient sunlight conditions. Carbon nanotube-delignified wood and carbon nanotubes-natural wood achieved 73 and 60% evaporation efficiencies, which were 12 and 18% more than that of wood only, respectively. This is due to the creation of huge micropores in the cell walls after the delignification process, promoting evaporation rate and water transportation to the top surface (He et al. 2019a, b).

A high-performance delignified and carbonized wood was also designed (Chen et al. 2019a, b). The delignification process increased water transfer capacity and lowered the thermal conductivity and heat loss in the wood structure. Improving the wood properties via the delignification process caused the photoabsorber to achieve an 89% efficiency under 1 sun. On the other hand, with the carbonization of the wood surface and designing the artificial channel-array, a refined wood-based photoabsorber with excellent antifouling properties was prepared. Due to high hydraulic conductivity, drilled channels acted as salt-rejection pathways and a

self-reconstructed photoabsorber was produced. This photoabsorber exhibited 75% evaporation efficiency under 1 sun (Kuang et al. 2019b).

To improve the evaporation efficiency, Zhang et al. treated lumens of wood by p-toluenesulfonic acid. The diameter of the wood lumens declined from 40 to 60 μm to 10–20 μm after treatment, and more hydrophilicity was observed in them. Under 1 sun, p-toluenesulfonic acid-wood photoabsorber achieved a flux of 2.2 kg m^{-2} h^{-1} and 87% evaporation efficiency (Zhang et al. 2020a, b, c). For improving interfacial solar steam generation, delignified wood was prepared and coated with Fe/Pd nanoparticles for designing single-layer photoabsorbers. A total of 103% enhancement was observed in interfacial solar steam generation under 3 sun using this photoabsorber. In addition, a double-layer photoabsorber composed of Fe/Pd nanoparticles and substrates of delignified wood and polystyrene foam was used with 83% evaporation efficiency under 3 sun (Ghafurian et al. 2020c).

A nanostructured biopolymer hygroscopic aerogel with a porous bilayer structure was prepared as a photoabsorber, comprised of a lithium chloride hygroscopic agent, a wood-derived nanofibrillated cellulose hydrophilic skeleton, and a graphene solar absorber. The photoabsorber achieved 90% evaporation efficiency under 3 sun (Wang et al. 2021a, b, c, d). To enhance the interfacial solar steam generation performance, several scalable techniques were used to modify the wood surface, including thermal carbonization, laser carbonization, coating wood with Au nanolayers, and combinations of these techniques. The wood coated with Au and subsequently carbonized with a hot plate obtained the highest evaporation flux of 4.02 kg m^{-2} h^{-1} at 3 sun among all prepared wood-based solar steam generation devices (Ghafurian et al. 2020b).

A wood modified by carbonization and coated with aluminophosphate could achieve efficiency and a flux of 90.8% and 1.423 kg m^{-2} h^{-1} under 1 sun, respectively (Chen et al. 2020). Fang et al. fabricated black woods using tannic acid and Fe^{3+} for interfacial solar steam generation. The photoabsorber exhibited 90% evaporation efficiency under 1 sun, excellent stability in acid or base media, and desirable oil-fouling performance (He et al. 2020).

Unrefined wood-based solar steam generation devices

A variety of the photothermal materials have been used as the top layer on the wood surface in wood-based solar steam generation devices, including metal nanoparticles, semiconductor, polymeric, carbon-based, and other nanomaterials. We summarize the various photothermal materials used in wood-based solar steam generation devices in Fig. 4.

Metal nanoparticles and semiconductor nanomaterials

Due to absorption of a wide range of solar spectrum, metal nanoparticles are considered as promising photothermal materials, and they have been widely used either as nanoparticles or hybrids and composites with other nanomaterials in wood-based solar steam generation devices. In metal nanoparticles, electromagnetic radiation is absorbed by stimulating the electrons from the conduction band to higher levels. When metal nanoparticles are irradiated, electrons are excited from occupied states to unoccupied states, resulting in the formation of hot electrons. The decay of hot electrons redistributes their energy, leading to a rapid rise in metal surface temperature (Gao et al. 2019a, b).

Plasmonic metal nanoparticles such as Au and Pd have been extensively used in photothermal applications because of their excellent light-to-heat conversion (Liu et al. 2017a, b, c; Zhu et al. 2018a, b). Chengmin et al. coated bamboo with noble metal nanoparticles and used it for interfacial solar steam generation desalination (Sheng et al. 2020). Benefiting from several microchannels, hydrophilicity, and low cost, bamboo serves as an excellent substrate for interfacial solar steam generation. Due to high optical absorptivity of plasmonic metal nanoparticles, plasmonic bamboo presented a maximum light absorption and showed 87% efficiency under 10 sun. Because of the plasmonic effect of the noble metal nanoparticles and open microchannels of wood, the plasmonic wood in other research showed high solar absorption with 85% evaporation efficiency at 10 sun (Zhu et al. 2018a, b).

However, interfacial solar steam generation devices composed of noble metal nanoparticles are much more expensive, and hence, they cannot be commercialized (Bae et al. 2015). In addition, most wood-based solar steam generation devices were unable to adsorb water pollutants, including heavy metal ions. For this reason, Mehrkhah et al. designed an efficient wood-based device consisting of wood coated with FeNi and reduce graphene oxide and used as a photoabsorber for interfacial solar steam generation and as a sorbent for heavy metal removal. The high evaporation flux of 1.50 kg m^{-2} h^{-1} was obtained at 1 sun (Mehrkhah et al. 2021a). Mehrkhah et al. also designed a cost-effective, non-noble wood-based device consisting of poplar wood coated with a FeNi/reduce graphene oxide nanocomposite, which was simultaneously used for seawater desalination and wastewater treatment. The as-prepared photoabsorber could achieve 90.23% evaporation efficiency under 1 sun which was comparable to that obtained using noble-metal wood-based devices and completely adsorb Pb (II) from aqueous solutions (Mehrkhah et al. 2021b).

A stable and efficient interfacial solar steam generation device was prepared by a flexible wood aerogel coated with

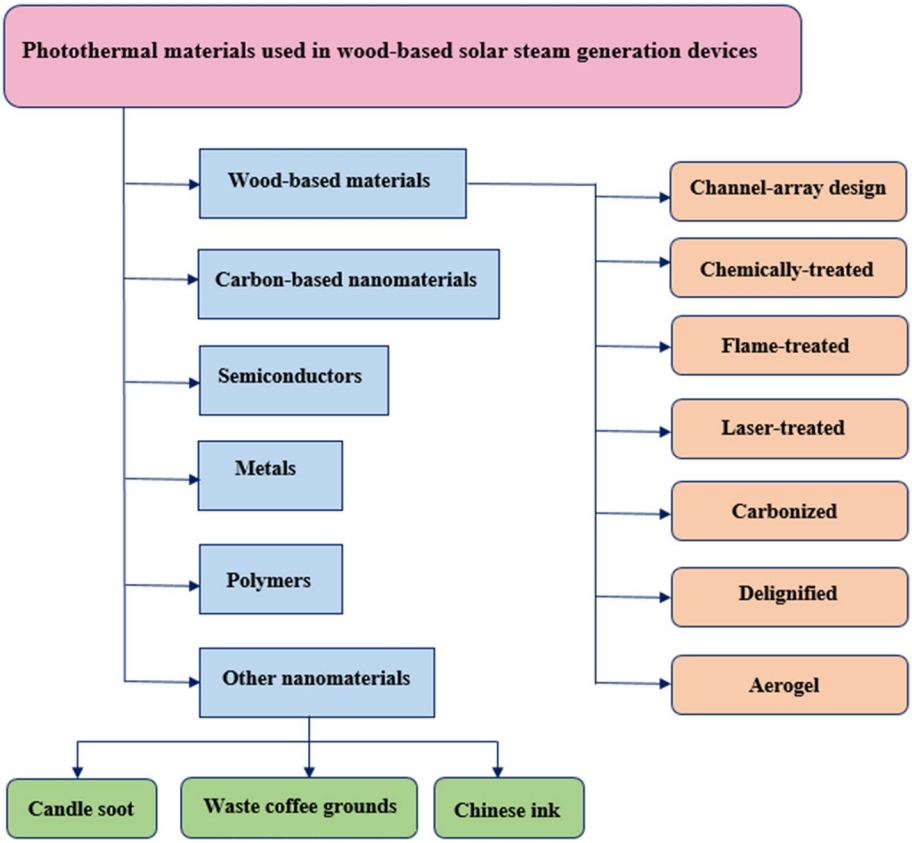

Fig. 4 Photothermal materials used in wood-based solar steam generation devices. Photothermal materials include wood-based materials, carbon-based nanomaterials, semiconductor nanomaterials, metal nanoparticles, polymeric nanomaterials, and other nanomaterials such as candle soot, waste coffee grounds, and Chinese ink. Wood-based materials used as a photothermal material in wood-based devices are achieved by treatment of wood surface, including carbonization, flame treatment, delignification process, laser treatment, chemically treatment, wood-based aerogel preparation, and channel-array design. Noble and nonnoble wood-based devices are composed of plasmonic metal nanoparticles such as Au and Pd due to their excellent light-to-heat conversion and nonnoble metal nanoparticles such as FeNi. Several semiconductor nanomaterials such as $CuFeSe_2$, VO_2, and black TiO_2 have been used in wood-based devices. Owing to low cost and high sunlight absorption, various carbon-based nanomaterials such as graphene oxide and carbon nanotubes have been extensively employed in wood-based devices. Polymeric nanomaterials, including polyethylene foam, polydopamine, and polypyrrole and other black nanomaterials such as candle soot, Chinese ink, and waste coffee grounds were deposited on the wood surface for preparation of wood-based devices

Au-reduce graphene oxide. The wood aerogel had a low thermal conductivity, light weight, and high hydrophilicity. The photoabsorber showed 1.394 kg m^{-2} h^{-1} flux under 1 sun. During 120-h interfacial solar steam generation, brine water was transported for evaporation during the day and salt residues were dissolved at night, reflecting the self-cleaning property of the photoabsorber (Qian Zhang et al. 2020a, b, c). Ebrahimi et al. coated pieces of poplar wood with Ag nanoparticles and reduce graphene oxide and used as a photoabsorber in the interfacial solar steam generation of seawater. Reduce graphene oxide/Ag/wood exhibited a high decrease in salinity and 5.99 kg m^{-2} h^{-1} evaporation flux under 3 sun (Ebrahimi et al. 2022). A double-layer photoabsorber was prepared by coating poplar wood by Ag and Pd nanoparticles, which achieved the high evaporation flux of 4.82 kg m^{-2} h^{-1} under 3 sun (Goharshadi et al. 2022).

Semiconductor nanomaterials exhibit unique size-dependent physical and chemical properties that differ from those of the bulk systems (Goharshadi et al. 2013a, b; Goharshadi et al. 2012, 2011). They have shown promising applications in different areas because of their facile synthesis, low-cost, fine-tunable absorption spectra, and large extinction coefficients in the near-infrared region (Gao et al. 2019a, b). Almost all semiconductor nanomaterials are in groups IV, III–V, and II–VI, including black TiO_2, MoS_2, NiO, and copper sulfides (Cu_2–S_x) (Ghim et al. 2018; Liu et al. 2017a, b, c; Song et al. 2018; Zhu et al. 2016a, b, c). When a semiconductor is irradiated, the electron–hole pairs are produced. The excited electrons eventually return to lower energy levels and release energy in the form of phonons (heat) (Gao et al. 2019a, b).

A solar absorber was introduced by coating the wood surface with $CuFeSe_2$ semiconductors with a narrow bandgap of 0.45 eV. The $CuFeSe_2$ wood showed a solar–thermal efficiency of 86.2% under 5 sun because of its excellent porous structure, low density, and the high hydrophilicity of wood (Liu et al. 2018a, b, c, d). A photoabsorber was designed by coating poplar wood with VO_2 and could achieve 75.60% evaporation efficiency under 3 sun (Aziznezhad et al. 2020). By coating the surface of wood with WO_{3-x} nanorod, a photoabsorber with 94.0% light absorption was reported. WO_{3-x} nanorod-coated wood could achieve an evaporation efficiency of 82.5% under 1 sun due to its excellent heat localization (Li et al. 2020). An efficient photoabsorber composed of wood coated with carbon nanotube and decorated by Fe_2O_3 nanoparticles (Fe_2O_3@carbon nanotube) was prepared. The wood/Fe_2O_3@carbon nanotube device achieved 1.42 kg m^{-2} h^{-1} interfacial solar steam generation flux under 1 sun (Li et al. 2021a, b, c, d).

Carbon-based and polymeric nanomaterials

Compared to metallic nanoparticles and semiconductor nanomaterials, carbon-based nanomaterials are cheaper and more abundant. Carbon-based nanomaterials also possess excellent sunlight absorption and high light-to-heat conversion efficiency (Gao et al. 2019a, b). One-dimensional to three-dimensional carbon-based structures have been fabricated as photothermal materials in wood-based solar steam generation devices.

Li et al. coated a graphene oxide film on the wood surface and used as an effective solar desalination photoabsorber. The photoabsorber showed an evaporation efficiency of 80% under 1 sun with four orders of salinity reduction (Li et al. 2016a, b). A photoabsorber composed of graphene-wood was also reported, exhibiting an interfacial solar steam generation efficiency of 91.8% under 1 sun (Kim et al. 2018). Li et al. used bamboo charcoal as an efficient interfacial solar steam generation device with porous structure. The bamboo charcoal evaporator showed a high evaporation efficiency of 84% under 1 sun and an excellent stability under acidic and alkaline conditions (Li et al. 2019a, b, c).

An efficient, hierarchical interfacial solar steam generator was prepared containing a light absorbing layer of carbon nanotubes/bacterial cellulose, a thermal insulation layer of glass bubbles/bacterial cellulose, and a wood substrate for supporting and transporting water. In interfacial solar steam generation, a cellulose nanofiber network of bacterial cellulose hydrogel significantly reduced vaporization enthalpy and a high evaporation flux of 2.9 kg m^{-2} h^{-1} and an efficiency of 80% were achieved (Fig. 5a) (Guan et al. 2020).

Polymeric nanomaterials are considered to be other photothermal materials used in wood-based devices. By imitating the water transfer of a tree, a solar absorber was designed consisting of air-laid paper as the tree root, polyethylene foam as the soil for decreasing the heat loss, and carbonized wood as the photothermal material. The solar absorber showed a high efficiency of 91.30% under 1 sun (Liu et al. 2018a, b, c, d). A polypyrrole-wood photoabsorber was prepared through the polymerization of pyrrole monomers into the wood structure. Due to the excellent light-harvesting of polypyrrole nanoparticles and the low thermal conductivity of wood, the polypyrrole wood achieved a high evaporation efficiency of 83% under 1 sun (Huang et al. 2019). An efficient wood-based evaporator consisting of natural phenolic substances and Fe^{3+} coordination exhibited an evaporation efficiency and flux of 54% and 0.92 kg m^{-2} h^{-1}, respectively (Gao et al. 2019a, b). A photoabsorber consisting of wood and arginine-doped polydopamine was synthesized, which could achieve 77% evaporation efficiency under 1 sun (Zou et al. 2021).

Other nanomaterials and reverse-tree design

Apart from four important types of photothermal materials, other nanomaterials are also used. For instance, a photoabsorber was designed composed of wood coated with candle soot. Due to the hydrophilicity and capillarity properties of wood as well as black candle soot surface, the as-prepared photoabsorber achieved a relatively high flux of 0.950 kg m^{-2} h^{-1} under 1 sun (Z. Wang et al. 2019a, b, c). Yang et al. coated Chinese ink on the wood surface and used it for interfacial solar steam generation applications (Yang et al. 2019a, b). The Chinese ink consisted of amorphous carbon nanoparticles and graphite-like nanoplatelets. The photoabsorber showed high absorption in a wide range of the solar spectrum and obtained a high evaporation efficiency of 82.2% under 1 sun.

Kim et al. prepared a cheap photoabsorber using waste coffee grounds deposited on a wood surface. The photoabsorber achieved an excellent absorption of sunlight (91%). The ball-milled activated waste coffee grounds-wood with excellent photothermal and antifouling properties exhibited evaporation fluxes of 1.45 kg m^{-2} h^{-1} under 1 sun for one cycle and 1.44 kg m^{-2} h^{-1} for 40 cycles (Kim et al. 2020a, b).

In the reverse-tree design, wood is vertically cut in the direction of tree growth, and hence, the pits are responsible for water transport to the surface of the wood-based solar steam generation devices (Li et al. 2018a, b, c, d). A wood-based device was fabricated consisting of graphite coated on vertically cut wood (Fig. 5b). The anisotropic thermal conductivity of wood along with a thin graphite layer led to the localization of solar energy at the evaporative surface. Nanoscale channels and a decoupled thermal transport direction in the wood structure resulted in crossplane

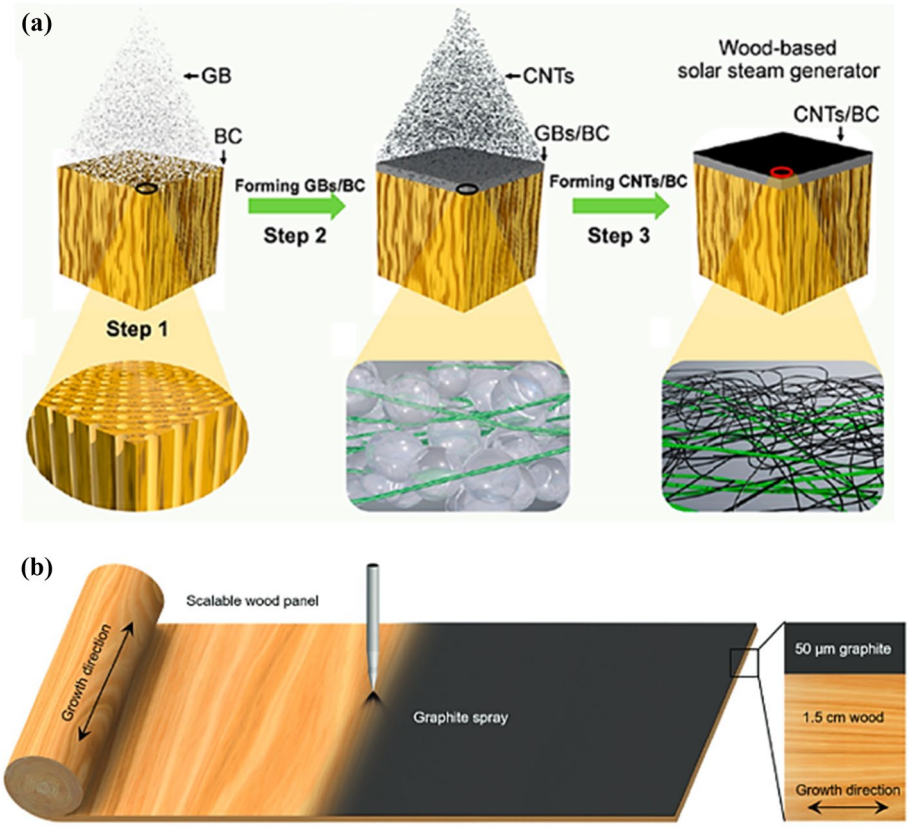

Fig. 5 **a** **P**reparation steps of a wood-based solar steam generator, including sunlight absorption layer and thermal insulating layer deposited on the wood substrate. In step 1, glass bubbles and bacterial cellulose were deposited on the wood so that in step 2, the thermal insulating layer of glass bubbles (GB) / bacterial cellulose (BC) was constructed. By embedding glass bubbles in the cellulose nanofiber network, an efficient thermal insulation layer with high capability of water transportation was formed. In step 3, carbon nanotubes (CNTs) / bacterial cellulose as a sunlight absorption layer was coated on the insolation layer by the process of aerosol-assisted biosynthesis. Reproduced with permission.(Guan et al. 2020) Copyright 2020, American Chemical Society. **b** Photoabsorber formed by vertically cut and spray-coated graphite mesoporous wood. In this work, by spray coating, a layer of graphite was spray-coated on the wood surface. The thicknesses of the graphite layer and wood substrate were chosen 50 μm and 1.5 cm, respectively, in order to achieve an efficient wood-based device. The low thermal conductivity of 0.11 W m^{-1} $K.^{-1}$ was measured for the vertically cut wood that is beneficial for heat loss prevention. The water was transported through pits and spirals in the vertically cut wood. The high evaporation efficiency of 80% was achieved under 1 sun. Reproduced with permission of Wiley from Li et al. (2018a, b, c, d)

water transfer and a decrease in heat loss. The photoabsorber exhibited a high evaporation efficiency of 80% under 1 sun and 89% under 10 sun (Li et al. 2018a, b, c, d).

In addition, through a reverse-tree design, He et al. prepared a photoabsorber by carbonization of a longitudinal wood surface. By reverse-tree design, water transport occurred via pits in the channels instead of the vessels and tracheids of wood. Due to broadband sunlight absorption by carbonized surface and the low thermal conductivity of longitudinal wood, the photoabsorber displayed a solar-to-thermal efficiency of 89% under 10 sun (Liu et al. 2018a, b, c, d). Table 2 summarizes the evaporative performance of several wood-based solar steam generation devices under different solar intensities.

Main factors affecting efficiency of wood-based solar steam generation devices

Several factors affect the efficiency of wood-based solar steam generation devices, including solar absorption, heat loss, photoabsorber geometry, pore radius, and ambient conditions.

Sunlight absorption

The solar spectrum is extremely important in interfacial solar steam generation efficiency. The sunlight absorption, α, by the photoabsorber is calculated by Eq. 11 (Yu et al. 2019):

Table 2 Evaporation performance of several wood-based solar steam generation devices under different solar intensities

Photoabsorber	Evaporation efficiency (%)	Sun (kW m^{-2})	References
Graphene oxide-wood	80.0	1	Li et al. (2016a, b)
Carbonized mesoporous wood	87.0	10	Zhu et al. (2017a)
Carbonized poplar wood	86.7	10	Jia et al. (2017b)
Flame-treated wood	72.0	1	Xue et al. (2017)
Flexible wood/carbon nanotubes	81.0	10	Chen et al. (2017a)
$CuFeSe_2$-wood	86.2	5	Liu et al. (2018a, b, c, d)
Paper-polyethylene-wood	91.3	1	Liu et al. (2018a, b, c, d)
Carbonized wood	91.3	1	Liu et al. (2018a, b, c, d)
Plasmonic wood	85.0	10	Zhu et al. (2018a, b)
Graphite-wood	80.0	1	Li et al. (2018a, b, c, d)
Carbonized longitudinal wood	89.0	10	Liu et al. (2018a, b, c, d)
Titanium nitride-carbonized wood	92.5	1	Guo and Yang, (2019)
Bamboo charcoal	84.0	1	Li et al. (2019b, c, a)
Carbon nanotube-delignified wood	73.0	1	He et al. (2019a, b)
Drilled/carbonized wood	75.0	1	Kuang et al. (2019b)
Polypyrrole-wood	83.0	1	Huang et al. (2019)
Delignified/carbonized wood	89.0	1	Chen et al. (2019a, b)
Candle soot-wood	59.0	1	Wang et al. (2019a, b, c)
Chinese ink-graphite-wood	82.2	1	H. C. Yang et al. (2019a, b)
Phenolic substance-Fe^{3+}	54.0	1	Gao et al. (2019a, b)
[a]Fe/Pd W5F5	78.0	3	Ghafurian et al. (2020c)
P-toluenesulfonic acid-wood	87.0	1	X. Zhang et al. (2020a, b, c)
Wood-tannic acid-Fe^{3+}	90.0	1	He et al. (2020)
Au-coated carbonized wood	83.5	1	Ghafurian et al. (2020b)
Wood@aluminophosphate	90.8	1	Chen et al. (2020)
[b] $CuCl_2$-carbon-PVDF/wood	98.0	1	Tian et al. (2020)
Titanium carbide-wood	96.0	1	Ma et al. (2020)
Graphene-wood-graphene	110.0	1	Huang et al. (2020)
Plasmonic bamboo	87.0	10	Sheng et al. (2020)
WO_{3-x} nanorod-wood	82.5	1	Li et al. (2020)
VO_2-poplar wood	75.6	3	Aziznezhad et al. (2020)
[c] BAWCG-wood	91.4	1	K. Kim et al. (2020a, b)
Reduce graphene oxide/FeNi composite-wood	90.2	1	Mehrkhah et al. (2021a)
Double-layer reduce graphene oxide/FeNi-wood	92.5	1	Mehrkhah et al. (2021b)

[a]Fe/Pd coated on the wood and polystyrene foam with a 5 mm diameter

[b]Copper chloride-carbon-polyvinylidene fluoride-wood

[c]Ball-milled activated waste coffee grounds

$$\alpha = \frac{\int \left(1 - R_f\right) \times q_s \times d\lambda}{\int q_s \times d\lambda} \tag{11}$$

where R_f is the reflectance of the photoabsorber's surface. q_s is solar intensity. λ stands for the wavelength.

Heat loss

Heat loss by the photoabsorber contains three parts, including radiation, conduction, and convection (Cui et al. 2018).

Radiation

Radiation loss is calculated using the Stefan–Boltzmann equation (Cui et al. 2018):

$$\Phi = \varepsilon A \Pi \left(T_1^4 - T_2^4\right) \tag{12}$$

where Φ is heat flux. ε stands for emissivity supposing that the evaporation has a maximum emissivity of 1. A is the photoabsorber surface area. Π is the Stefan–Boltzmann constant (5.6703×10^{-8} W m^{-2} K^{-4}). T_1 is the surface temperature of the photoabsorber under solar illumination. T_2 is the environment temperature.

Conduction

Conduction heat loss referring to the heat from the photoabsorber to bulk water is calculated by Eq. 13 (Cui et al. 2018):

$$\varphi = Mc\Delta T \tag{13}$$

where φ is the conduction heat energy loss, and c is the specific heat capacity of pure water (4.2 kJ K^{-1} kg^{-1}). M is the bulk water weight and ΔT is the temperature change of the bulk water after evaporation. The relationship between resistance to heat conduction and thickness of the photoabsorber is expressed with the following equation (Cui et al. 2018):

$$\Omega = \frac{v}{TC \times A} \tag{14}$$

where Ω is resistance to heat conduction, and v is the thickness of wood-based solar steam generation devices. TC stands for the thermal conductivity.

Convection

Convection heat loss is calculated using Newton's law of cooling (Cui et al. 2018):

$$\Lambda = HA\Delta T \tag{15}$$

where Λ is heat transfer rate. H is the convection heat transfer coefficient. A is the photoabsorber surface area.

Photoabsorber geometry

The hydrophilicity of photoabsorbers is also of great importance due to the pumping of water from the bulk to the evaporative surface. However, high hydrophilicity causes the heat generated to be lost to the underlying water. Adjusting the geometry of wood can tune the hydrophilic effect by governing the amount of surface water. The evaporation efficiency of a photoabsorber depends on its geometry (Yu et al. 2019). Photoabsorber efficiency is calculated using both thermal efficiency and maximum water-transfer efficiency. The thermal efficiency, η_1, of the photoabsorber is calculated using Eq. 16 (Yu et al. 2019):

$$\eta_1 = \left(\propto - \frac{\varepsilon \Pi \left(T_1^4 - T_0^4\right)}{q_s} - \frac{H\left(T_1 - T_0\right)}{q_s} - \frac{\varphi}{q_s} \right) \times 100\% \tag{16}$$

where H is the convection heat transfer coefficient. φ is the conduction heat loss of the photoabsorber (W m^{-2}). q_s is solar irradiation, Π is the Stefan–Boltzmann constant (5.6703×10^{-8} W m^{-2} K^{-4}), ε is the emissivity of the photoabsorber surface (Ni et al. 2016), β_0 is the initial temperature of the surroundings, and β_1 is the final temperature of the photoabsorber surface after irradiation.φ is calculated by Eq. 17:

$$\varphi = \frac{\left(T_1 - T_0\right)}{\frac{v}{TC_p} + \frac{Z_0}{TC_w}} \tag{17}$$

where ν is the photoabsorber thickness, TC_p is the thermal conductivity of the photoabsorber, and Z_0 is the distance between the bottom part of the container and the bottom of the photoabsorber. TC_w is the thermal conductivity of water. According to Eq. 17, Eq. 16 is expressed as Eq. 18:

$$\eta_1 = \alpha - \frac{\varepsilon \Pi \left(T_1^4 - T_0^4\right)}{q_s} - \frac{v\left(T_1 - T_0\right)}{q_s} - \frac{\left(T_1 - T_0\right)}{\left(\frac{v}{TC_p} + \frac{Z_0}{TC_w}\right) q_s} \times 100\% \tag{18}$$

The maximum efficiency of water transfer, η_2, by a photoabsorber is calculated using Eq. 19 (Yang et al. 2018a, b):

$$\eta_2 = \frac{h_{Lv} \dot{m}_f}{q_s} \times 100\% \tag{19}$$

where $\dot{m}_f$ is the evaporation flux. h_{Lv} stands for the total evaporation enthalpy of water. q_s is solar irradiation.

The water flow flux ($\dot{m}_f$) of the evaporator with different thicknesses is obtained using Eq. 20:

$$\dot{m}_f = \frac{\rho \sigma \phi d}{4 \tau \mu v} \tag{20}$$

where ρ is the water density. ϕ is porosity of the wood (%). σ denotes the surface tension of water, d is the diameter of the microchannels, and μ is the fluid viscosity. τ is the microchannels tortuosity in the photoabsorber.v is the thickness of the photoabsorber. Hence, the maximum water-transfer efficiency of the photoabsorber, η_2, is calculated through Eq. 21 according to Eqs. 19 and 20:

$$\eta_2 = \frac{\rho \sigma \phi d}{4 \tau \mu v} \times \frac{h_{lv}}{q_s} \times 100\% \tag{21}$$

where h_{Lv} stands for the total enthalpy of the water evaporation. According to Eqs. 18 and 21, the minimum between η_1 and η_2 in the curve of efficiency vs. thickness gives the optimum thickness of the wood substrate that is crucial to achieve high evaporation efficiency (Fig. 6a) (Yu et al. 2019).

Heat transfer analysis also confirms the need for optimum thickness in the wood substrate. A carbonized wood with several heights of 1, 3, and 7.5 cm were prepared, and their evaporation fluxes were compared under 1 sun. As the height increased (7.5 cm), a thinner water film formed on the photoabsorber surface indicating that a thick solar absorber may not be favorable. More heat loss through convection and radiation also occurred as the surface temperature of the carbonized wood increased. On the contrary, the thin evaporator (1 cm) dissipated the heat to the bulk water by conduction loss. As a result, carbonized wood with a 3-cm thickness exhibited the highest evaporation flux due to the establishment of a trade-off between the amount of surface water and surface temperature (Zhang et al. 2019).

Pore radius

The pore radius of the wood-based solar steam generation devices can affect evaporation enthalpy. According to classical thermodynamic theory, energy transition during water evaporation is represented by a change in enthalpy (Tian et al. 2020):

$$\Delta_{vap}H_m = H_g - H_l \tag{22}$$

where H_g and H_l are the enthalpy of the gas and liquid phase, respectively. The enthalpy is defined as follows:

$$H = E + PV \tag{23}$$

where E is internal energy. V is the volume and P stands for the pressure. Hence, gas phase enthalpy and liquid phase enthalpy can be calculated using the following:

$$H_g = E_g + P_g V_g \tag{24}$$

$$H_l = E_l + P_l V_l \tag{25}$$

where P_g, V_g, P_l, V_l are the pressure and volume of gas phase and liquid phase, respectively. The internal energy of matter can be expressed as follows:

$$E = E_k + U = E_k + U^{intra} + U^{inter} \tag{26}$$

where U^{intra} and U^{inter} are intramolecular and intermolecular potentials, respectively. By substituting Eq. 26 in Eqs. 24 and 25, the following equations are obtained:

$$H_g = E_{kg} + U_g^{intra} + U_g^{inter} + P_g V_g \tag{27}$$

$$H_l = E_{kl} + U_l^{intra} + U_l^{inter} + P_l V_l \tag{28}$$

where E_{kg} and E_{kl} are the kinetic energy of the gas and liquid phases, respectively. $U_g^{intra}, U_l^{intra}, U_g^{inter}, U_l^{inter}$ are intramolecular and intermolecular potentials for gas and liquid phases, respectively.

Accordingly, Eq. 22 can be written as follows:

$$\begin{aligned}\Delta_{vap}H_m = &\left(E_{kg} - E_{kl}\right) + \left(U_g^{intra} - U_l^{inter}\right) \\ &+ \left(U_g^{inter} - U_l^{inter}\right) + \left(P_g V_g - P_l V_l\right)\end{aligned} \tag{29}$$

Water vapor is considered as an ideal gas because its intermolecular potential is negligible at 1 atm. Therefore, Eq. 29 can be written as follows:

$$\Delta_{vap}H_m = \left(E_{kg} - E_{kl}\right) + \left(U_g^{intra} - U_l^{inter}\right) - U_l^{inter} + \left(nRT - P_l V_l\right) \tag{30}$$

where R is gas constant. T stands for the absolute temperature. Whether in the liquid phase or in the gas phase, kinetic energy ($E_{kg} - E_{kl} = 0$) and the vibrational energy of bonds ($U_g^{intra} - U_l^{inter} = 0$) is almost the same. In the calculation of molar phase change enthalpy, the amount of matter is $n = 1$. Therefore, the calculation formula for evaporating enthalpy is obtained:

$$\Delta_{vap}H_m = -U_l^{inter} + \left(RT - pV_l\right) \tag{31}$$

where U_l^{inter} denotes the liquid water intermolecular potential. V_l is the volume of the liquid water. Based on pressure caused by the surface tension,P, which is calculated by Eq. 6, Eq. 31 can be rewritten as follows (Hou et al. 2019):

$$\Delta_{vap}H_m = -U_l^{inter} + \left[RT - \left(P + \frac{4\sigma cos\theta}{r}\right)V_l\right] \tag{32}$$

where σ is the surface tension. θ stands for the contact angle. r is the pore size. Based on this equation, $\Delta_{vap}H_m$ depends on the radius of the pore. The relationship curve between pore size and ΔH_v is illustrated in Fig. 6b for 1 mol of water at 298 K and $\sigma = 0.072$ N m^{-1}, and $\theta = 0$. The$\Delta_{vap}H_m$ value decreases with the reduction of pore size.

Ambient conditions

Ambient conditions, including water depth, relative humidity, and the salinity of the water, influence the evaporation efficiency of wood-based solar steam generation devices.

Water depth

A synergistic effect between surface temperature and the thickness of surface water is achievable for obtaining maximum evaporation efficiency. Since wood-based solar steam

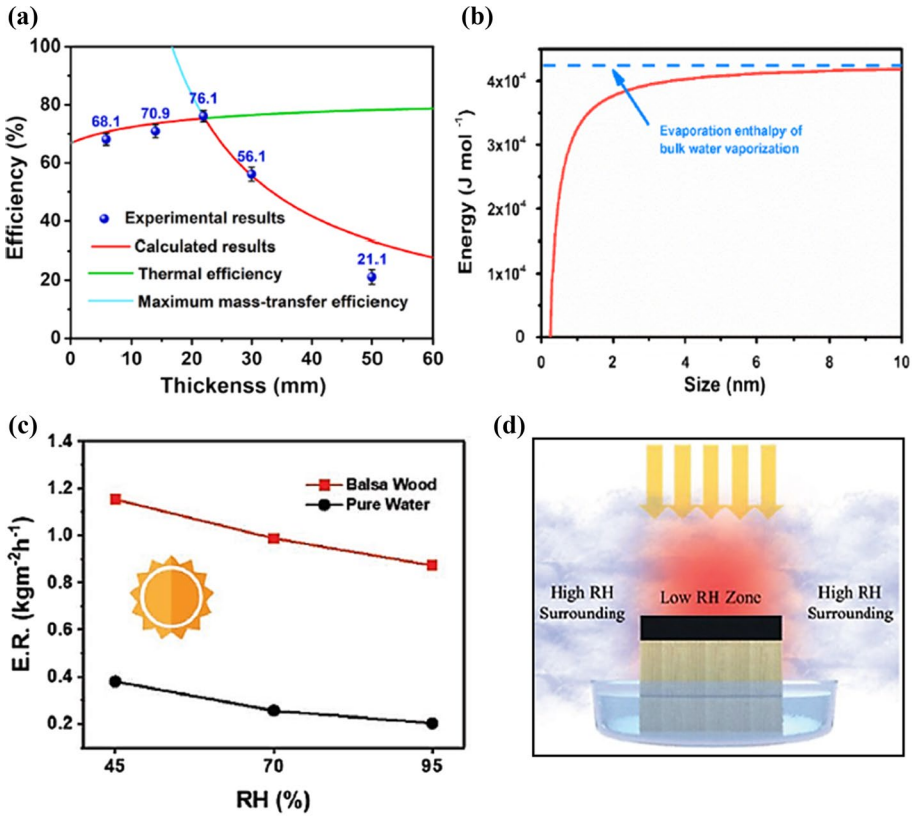

Fig. 6 **a** Relationship between photoabsorber efficiency and the thickness. The red line is the maximum efficiency of the photoabsorber calculated based on the maximum mass-transfer efficiency denoted as cyan line and the thermal efficiency denoted as green line. The blue circles show the photoabsorber efficiency measured under 1 sun in the experiment. Evaporation efficiency increased from 68.1% to 76.1% with increasing the photoabsorber thickness from 6 to 22 mm. The photoabsorber efficiency decreased to 21.1%, when the thickness exceeded 50 mm. Therefore, the optimal thickness is 22 mm so as to achieve the maximum evaporation efficiency. These results were consistent with those of the experimental studies. Reproduced with permission of Elsevier from Yu et al. (2019). **b** Dependence of the water evaporation enthalpy on the diameter of the pores of $CuCl_2$-activated pollen cell photoabsorber. The value of evaporation enthalpy for water decreased with a reduction in the pore size. The most decrease in the enthalpy is observed in the diameter of 2 nm, where molecules of water are confined in the photoabsorber with 1 nm pores. Reproduced with permission of Wiley from Tian et al. (2020). **c** Evaporation rate (ER) under light illumination and ambient relative humidity (RH). Evaporation rate of a balsa wood-based device was measured under 45%, 70%, and 95% ambient relative humidity. The results showed that by increasing the relative humidity even up to nearly 100%, no significant reduction in the evaporation rate was observed under light. **d** Low- relative humidity area near hot evaporative surface. Due to formation of a low-relative humidity area near the evaporation surface imposing a more effect on the evaporation rate with respect to the surrounding, relative humidity of ambient plays a minor role in solar steam generation. Reproduced with permission of Wiley from Zhang et al. (2019)

generation devices divert water to the evaporative surface through a capillary effect, they can maintain a proper height difference between the surface, which is irradiated, and water depth. Moreover, by changing pore size, optimum performance of wood-based solar steam generation devices can be obtained (Kaur et al. 2019).

Relative humidity

Because a strong interaction between the photoabsorber and the ambient plays an important role in evaporation efficiency, the relative humidity of the ambient may not be an accurate characteristic for representing the actual humidity level of wood-based solar steam generation devices. For example, the evaporation flux of carbonized wood was measured under several ambient relative humidity (45%, 70%, and 95%). The results revealed that evaporation flux did not decrease significantly under light even under high ambient relative humidity (95%) (Fig. 6c), whereas the photoabsorber performance in the dark decreased as relative humidity increased, indicating that dark evaporation is strongly influenced by the ambient relative humidity (Zhang et al. 2019).

A low-relative humidity area is generated near the hot evaporative surface which is more influential in the evaporation with respect to the ambient relative humidity (Fig. 6d). Consequently, ambient relative humidity has a negligible

impact on solar evaporation. The relative humidity of this specific area is controlled by the temperature of the illuminated evaporative surface. This temperature plays a major role in evaporation efficiency so that it should be considered for the heat loss calculations instead of the ambient temperature (Yang et al. 2018a, b).

Water salinity

Water with high salinity may have a noticeable effect on the evaporative performance of wood-based solar steam generation devices, while salt formation on the evaporation hot surface significantly weakens the continuous evaporation regardless of the long refresh time (Yin et al. 2017; Zhu et al. 2018a, b).

Stability of wood-based solar steam generation devices

The long-term stability of wood-based solar steam generation devices is of great importance in practical applications. There are several ways to evaluate the stability and durability of wood-based solar steam generation devices.

One way to evaluate the stability of wood-based solar steam generation devices is to investigate their performance under harsh conditions, including strong acidic and alkali media, high temperature or long sonication time. The flexible-wood/carbon nanotubes photoabsorber was exposed under different harsh actions such as folding and twisting in the water. In addition, the photoabsorber was soaked in the harsh conditions of acidic, alkali, and high temperature for 24 h, and no leakage of carbon nanotubes was observed showing the excellent stability of the structure of flexible-wood/carbon nanotubes (Chen et al. 2017a).

A plasmonic wood consisting of wood coated with noble-metal nanoparticles presented an excellent stability in pure, acid, and alkaline water. The stability of plasmonic wood was also examined under ultrasonication for 30 min in neutral, acidic, and alkaline aqueous solutions. No nanoparticles were found in aqueous solutions, indicating the stability of the photoabsorber during ultrasonication time (Zhu et al. 2018a, b). Polypyrrole wood was immersed under harsh conditions (acid, alkaline, high temperature, and sonication) for 2 h. Under these conditions, polypyrrole wood did not change, showing that the photoabsorber is stable and suitable for practical interfacial solar steam generation applications (Huang et al. 2019).

To evaluate the stability of wood coated with natural phenolic compound-iron complexes, its photothermal effects were investigated under acidic (pH 4.2), neutral (pH 7), and basic (pH 9.3) conditions. The photothermal properties of the as-prepared photoabsorber were very similar under different pHs and did not obviously change after 1 h showing good photothermal stability of the photoabsorber (Gao et al. 2019a, b).

A photoabsorber composed of Pd/bamboo was also stable in acid and alkaline water even after 30-min ultrasonication. Pd nanoparticles were attached well to wood due to their electrostatic attractions with hydroxyl functional groups of wood vessels (Sheng et al. 2020). The structural stability of a solar evaporator prepared by coating MnO_2 nanoparticles on $KMnO_4$ oxidized wood was investigated in several harsh environments, including acid and alkaline solutions for 24 h as well as ultrasonic treatment for 2 h. The evaporator retained its black appearance, and there was no obvious change in its structure. In addition, its evaporation performance did not change under harsh conditions (Fig. 7a, D. Li et al. 2021a, b, c, d).

A durability test is another way to assess the stability of a photoabsorber. The interfacial solar steam generation experiments were performed on carbonized wood for 100 h under 5 sun, and the results were verified stability and scalability of the photoabsorber for long-term applications (Zhu et al. 2017a). The stability test was also performed on a graphite-coated wood for 50 cycles (30 min for each cycle) under 1 sun. The results showed no noticeable change in photoabsorber performance (Li et al. 2018a, b, c, d). The WO_{3-x}-wood photoabsorber was used in interfacial solar steam generation experiments for 60 cycles under 1 sun. The evaporation flux of the photoabsorber remained unchanged after 60 cycles indicating the excellent durability of the photoabsorber (Li et al. 2020).

The durability test was also performed for waste coffee grounds wood. It was observed that the evaporation flux of the photoabsorber remained without any changes during 40 cycles (Kim et al. 2020a, b). The durability of the arginine-doped polydopamine-wood composite was investigated by performing interfacial solar steam generation experiments during 100 cycles. There was no obvious decrease in the water evaporation flux within these cycles. In addition, arginine-doped polydopamine-wood remained stable without obvious peeling and change of its shape (Zou et al. 2021). The stability of a delignified wood coated with Fe_3O_4 nanoparticles was investigated by immersing in 3.5 wt% NaCl solution for 120 h. The results showed that no salt was deposited on Fe_3O_4-delignified wood (Song et al. 2021).

A low-cost, scalable wood oxidized by $KMnO_4$ ($KMnO_4$-wood) was introduced for interfacial solar steam generation, which showed high evaporation performance and structural stability. The cycling performance of $KMnO_4$-wood in the seawater showed that it still remains stable even after 20 cycles under 1 sun (Fig. 7b) (Li et al. 2021a, b, c, d). Cyclic stability of a carbonized bamboo was investigated by immersing it in contaminated water for 60 cycles. After 60 cycles, evaporation flux and efficiency were

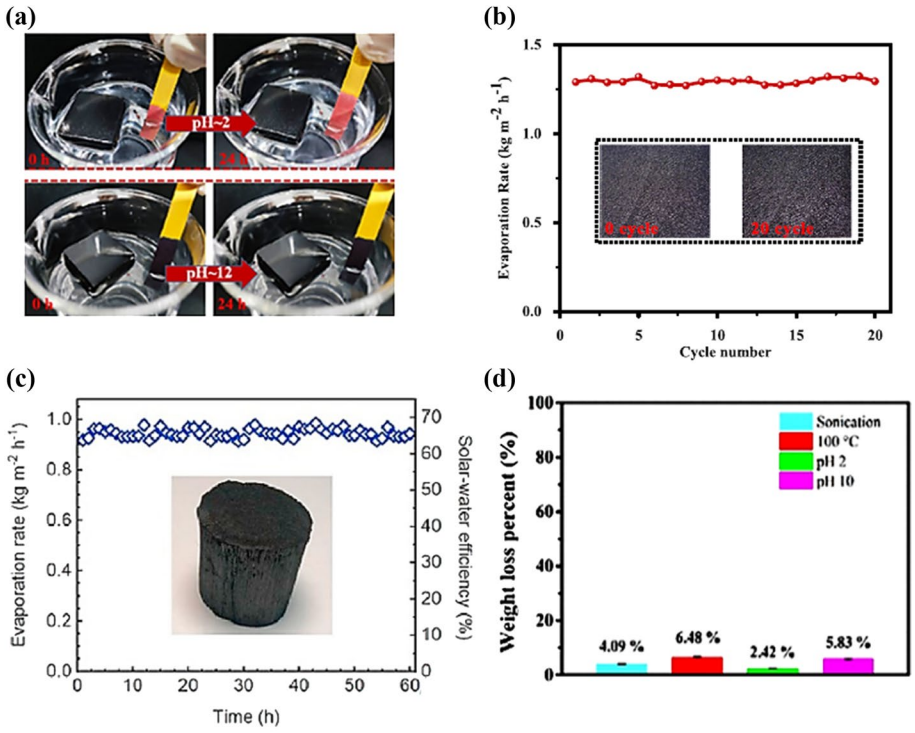

Fig. 7 **a** Stability of the $KMnO_4$-wood under harsh environments before and after immersing in the acid solution (pH 2) and alkaline solution (pH 12) for 24 h. The $KMnO_4$-wood remained unchanged after this period, and no difference was observed in its black appearance and structure before and after 24 h. **b** Evaporation rate of the $KMnO_4$-wood for 20 cycles in seawater (the inset shows the $KMnO_4$-wood images before and after cycling test). The cycling evaporation performance of the $KMnO_4$-wood demonstrates the evaporation rate achieved by the photoabsorber (1.28 kg m^{-2} h^{-1} under 1 sun) did not change after 20 cycles without any degradation displaying the photoabsorber is stable. Reproduced with permission of ACS from Li et al. (2021a, b, c, d). **c** Cyclic performance of carbonized bamboo in the seawater over 60 h (inset illustrates the carbonized bamboo image after 120-h solar desalination of contaminated water and seawater). There is no difference in the evaporation rate and efficiency after 60 cycles (1 h for each cycle). No damage is also observed in the carbonized bamboo structure after 60 h reflecting the cyclic stability of the photoabsorber. Reproduced with permission of Elsevier from.Gong et al. (2021). **d** Weight loss of the polypyrrole-wood device under harsh conditions for 2 h (strong acid, strong alkali, high temperature, and sonication conditions). With a negligible weight loss after subjecting to harsh conditions, the polypyrrole-wood exhibited excellent structural stability that is beneficial for practical applications. Reproduced with permission of RSC from Huang et al (2019)

very close to those of the initial cycle (Fig. 7c) (Gong et al. 2021).

A photoabsorber made by hydrophobic polyethylene wrapped by wood cellulose aerogel and coated with a double layer of hydrophobic soot-coated cloth/hydrophilic cloth represented an evaporation flux of 1.277 to 1.314 kg m^{-2} h^{-1} after continuous interfacial solar steam generation for 10 h (Peng et al. 2021). A solar evaporator with an excellent self-cleaning property was prepared by cutting out the artificial channel and polymerizing polypyrrole on the wood surface. The efficiency of the evaporator did not change obviously after continuous illumination under 1 sun for 30 h in a solution of 3.5 wt% NaCl and after 40 h in a solution of 20 wt% NaCl reflecting its stable performance in high-concentration saline solutions (Lei et al. 2021).

Continuous water evaporation in closed devices results in a gradual increase of water salinity in practical applications. Hence, it is necessary to investigate the performance of wood-based solar steam generation devices in the NaCl solutions with higher salinities than that of the seawater in order to evaluate their stability with an increase in water salinity.

He et al. showed a bimodal photoabsorber with an interconnected and porous microstructure. The photoabsorber showed excellent stability in a 15 wt% NaCl solution with an evaporation flux of 6.4 kg m^{-2} h^{-1} under 6 sun, demonstrating that it could be used for long-term desalination with a high salinity. In fact, brine diffusion via pits, tracheids, and vessel channels could prevent accumulation of the salt on the evaporative surface (He et al. 2019a, b).

A photoabsorber was designed with excellent salt resistance through depositing graphitic carbon layers on a wood surface by a CO_2 laser. A 20 wt% NaCl solution was used for desalination, and the photoabsorber could maintain the salt resistance even after 2 weeks of continuous evaporation,

indicating excellent performance of the photoabsorber in long-term desalination (Jang et al. 2020).

The mass loss percent of a photoabsorber is calculated using Eq. 33 in order to analyze the stability (Zhu et al. 2018a, b):

$$m_l\ \% = \left(\frac{m_b - m_a}{m_b}\right) \times 100 \tag{33}$$

where m_l represents weight loss, m_a is dry weight after immersion, and m_b stands for dry weight before immersion. Huang et al. performed the stability analysis (Fig. 7d). As illustrated, the photoabsorber shows low mass loss percentages even under strong acid and alkali, high temperature, and sonication conditions (Huang et al. 2019).

Challenges

Biofouling

Although wood as a biocompatible substrate is beneficial in interfacial solar steam generation systems, it is vulnerable to biofouling and biodegradation, thus affecting the long-term performance of the photoabsorber (Huang et al. 2020). Considerable efforts have been devoted to designing highly efficient and durable wood-based solar steam generation devices with excellent pathogen resistance (Huang et al. 2019).

When wood is floating on saline water for a long time, it becomes easily mildewed and fragmented, leading to low durability of wood-based solar steam generation devices. Due to long-term floating, a dense film of pathogens covers all of the surface of wood caused by bacteria growth and accumulation in biomass under a high-humidity condition. It results in the blockage of active sites of the sunlight absorption, which decreases the effective evaporative surface area of wood-based solar steam generation devices (Sun et al. 2020a, b). Hence, the internal structure of wood and its composition should be adjusted to prevent the formation of pathogens.

There are several solutions to remove biofouling formation:

1. Noble metal nanoparticles, such as Ag nanoparticles as photothermal materials, can be used because they have strong antibacterial activity (Gu et al. 2021; Slavin et al. 2017). Ag nanoparticles can attach to the cell membrane and disturb its performance (Moghayedi et al. 2017b). The membrane of a bacterial cell is damaged by the bactericidal effect of Ag ions and Ag nanoparticles (Zuo et al. 2020). The strong interaction between Ag^+ or Ag nanoparticles and thiol groups in the enzyme of a bacterial cell causes cell death (Slavin et al. 2017).

   The antibacterial activity of Ag-polydopamine@wood photoabsorber was examined against *Escherichia coli*. Culturing *Escherichia coli* suspension with Ag-polydopamine@wood for 24 h completely killed the bacteria. Instead, the number of *Escherichia coli* bacteria suspension cultured with raw wood did not change after this time (Yang et al. 2020). The antibacterial activity of poplar wood coated with reduce graphene oxide/Ag was investigated against *Staphylococcus aureus* compared to natural wood. The bacterial growth was totally inhibited even at the beginning of the exposure to reduce graphene oxide/Ag. On the contrary, bacterial growth was not inhibited by natural wood even after elapsing 24 h (Ebrahimi et al. 2022).
2. Metal oxide nanoparticles, such as ZnO, Fe_2O_3 nanoparticles or other nanomaterials, produce reactive oxygen species, including hydroxyl radicals (OH^o), hydrogen peroxide (H_2O_2), and singlet oxygen ($^1O_2$) through the interaction between the cell wall of bacteria and nanomaterials, and therefore, they could be utilized as anti-bacterial photothermal materials (Jalal et al. 2010; Moghayedi et al. 2020, 2017a; Rufus et al. 2016). The reactive oxygen species production results in the death of bacteria owing to enzymes inactivation and the peroxidation of lipid (Fang et al. 2006; Jones et al. 2008).

   The excellent antibacterial properties of carbon nanotube/wood aerogel are due to reactive oxygen species production. Carbon nanotube/wood aerogel and *Escherichia coli* culture medium were placed in a sealed container and exposed to near-infrared irradiation to produce a large amount of reactive oxygen species. After 24 h, a large amount of *Escherichia coli* bacteria were killed, representing the large amount of reactive oxygen species released by carbon nanotube/wood aerogel assisted by near-infrared irradiation (Kim et al. 2020a, b).
3. The other way to address this challenge is to use an aerogel wood as a wood-based solar steam generation substrate. Wood aerogel not only has the properties of natural wood, such as hydrophilicity, light weight, and low thermal conductivity, but also inhibits pathogen film formation and fragility, resulting in the long-lasting stability of wood-based solar steam generation devices. Wood aerogel is made of a lamellar structure with well-ordered cavities. In addition, starch and monosaccharides needed for pathogens' survival are chemically removed during the aerogel preparation, which helps wood-based aerogel develop a pathogen-resistant and self-cleaning property and exhibit long-term stability (Qian Zhang et al. 2020a, b, c).

For instance, no pathogen was grown on the photoabsorber surface of the Au-reduce graphene oxide/wood-based aerogel in comparison with that of moldy Au-reduce graphene oxide/wood, exhibiting an excellent pathogen-resistant property among wood aerogels (Zhang et al. 2020a, b, c). To examine the biological stability of natural wood and a thermally stable wood-derived aerogel (prepared via the delignification process and thermal treatment), they were placed on the water surface. Many pathogens covered the wall of tracheids in the natural wood after 60 h under 1 sun, indicating that the wood was infected by fungus (Fig. 8a). The surface and inside of thermally stable wood-derived aerogel had no obvious pathogen aggregation with respect to that of moldy wood photoabsorber (Fig. 8b). Due to thermal treatment and removal of pathogens' nutrients, such as starch and monosaccharides from wood, pathogen resistance of thermally stable wood-derived aerogel increased (Meng et al. 2021).

4. Another way to reduce pathogen deposition on wood-based solar steam generation devices is using graphene in the photoabsorber structure. Owing to the sharp edges that are able to break the integrity of the cell membrane, graphene has excellent antibacterial capacity (Akhavan and Ghaderi, 2010; Moghayedi et al. 2017b; Wilson et al. 2020).

Huang et al. prepared an interfacial solar steam generation device, namely laser-induced graphene wood. This device was composed of three layers, including a superhydrophilic laser-induced graphene as a bottom layer for rejecting lipophilic organic materials, wood as a middle layer for water transfer, and a hydrophobic laser-induced graphene as a top layer for the prevention of salt accumulation. The presence of oxygen functional groups in the laser-induced graphene bottom layer significantly reduces wood decomposition and biofouling by bacteria. The scanning electron microscopy images show that more *Escherichia coli* grows on the wood surface with respect to laser-induced graphene wood (Fig. 8c, d) (Huang et al. 2020).

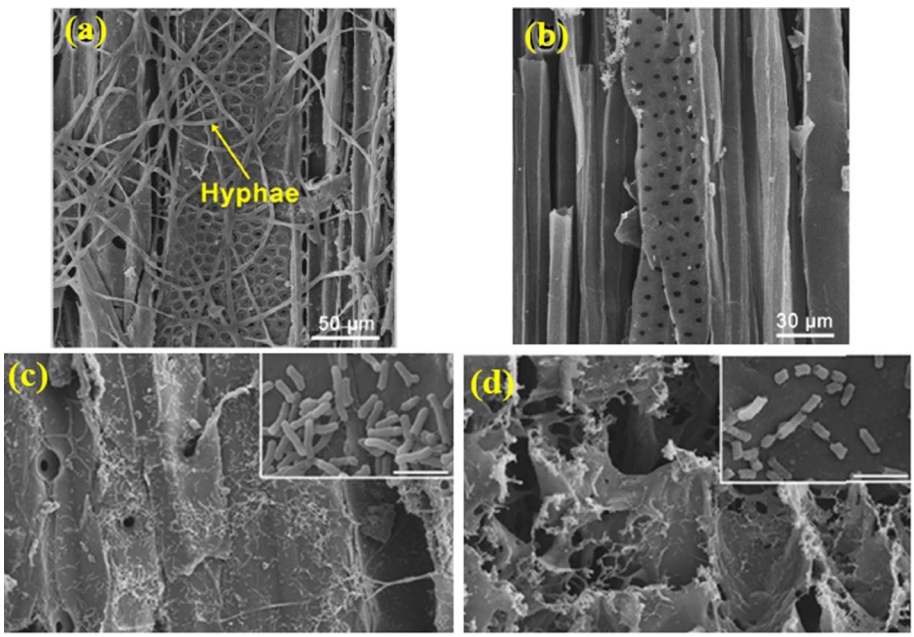

Fig. 8 Morphology of the surface of **a** natural wood and **b** thermally stable wood-derived aerogel after floating on the river for 60 h continuous solar illumination. After this period, a lot of mildew was located in the pores of wood so that the tracheids wall was covered with numerous hyphae. After subjecting to harsh conditions, including high humidity, bacteria accumulated in the wood microchannels leading to an infection of wood. In contrast, there is no significant mildew accumulation in the thermally stable wood-derived aerogel. This is because the nutrients needed for mold grow, including monosaccharides and starch, were removed by thermal treatment. Reproduced with permission of Elsevier from Meng et al. (2021). Scanning electron microscopy images of **c** the wood and **d** laser-induced graphene-wood after biofilm fixation. The insets show the structure of *Escherichia coli* accumulated on the wood and the photoabsorber's surface. The scale bars in figures **c** and **d** are 50 μm (the inset scale bars are 3 μm). The presence of more *Escherichia coli* grown on the surface of wood compared to laser-induced graphene-wood reveals that many oxygenated functional groups in bottom layer of this photoabsorber help to reduce wood biofouling. The structure integrity of bacteria cell on the wood surface was maintained while fragmenting the bacteria cells on the laser-induced graphene-wood implies that bactericidal properties of the photoabsorber causing the bacteria to be nonviable. Reproduced with permission of ACS from Huang et al. (2020)

Salt fouling

Although numerous efforts have been performed to increase the evaporation efficiency of wood-based solar steam generation devices, little attention has been paid to their long-lasting stability (Zhang et al. 2020a, b, c). Salt fouling can block sunlight and water transport to the surface, leading to a decrease in evaporation efficiency. Therefore, the accumulation of salt on the evaporative surface of wood-based solar steam generation devices is a big challenge and the practical use of wood-based solar steam generation devices can be limited by salt fouling (Wu et al. 2021). The fast water loss from the vaporization interface results in a significant increase and saturation of salt concentration on the evaporative surface of the photoabsorber.

The deposited salt causes the water transfer paths to gradually block, leading to reduction of steam generation (Fig. 9a, b) (Finnerty et al. 2017; Li et al. 2016a, b; Ni et al. 2018; Xu et al. 2018). As these figures show, small channels (i.e., tracheids) are first blocked after 0.5 h because of insufficient replenishment of the brine, and then, the salt gradually extends to the whole surface after 1 h. Hence, it is necessary to remove the salt accumulated through post-treatments in order to use wood-based solar steam generation devices for several cycles. Although the backwashing technique is a proper method for flexible membranes, removing the salt accumulation certainly increases the cost (Jin et al. 2018; Kou et al. 2019; Li et al. 2019b, c, a; Ren et al. 2017). Therefore, wood-based devices with salt-fouling properties are highly desired (Kuang et al. 2019b).

The amount of accumulated salts from the evaporation flux can be calculated by Eq. 34 for a solar evaporation device (Lee et al. 2020):

$$m_s = m_w\left(1 \cdot 52 \times 10^{-4} S^2 + 9 \cdot 50 \times 10^{-3} S\right) \tag{34}$$

where m_s is the precipitated salt mass, m_w denotes the evaporated water mass, and S stands for the initial salt concentration of the brine in wt% NaCl.

There are several solutions for addressing this problem:

1. Designs of wood-based solar steam generation devices with a hydrophobic membrane are considered to be effective solutions in reducing salt accumulation during interfacial solar steam generation (Hao et al. 2018; Y. Yang et al. 2019a, b; J. Zhao et al. 2018a, b, c). A hydrophobic surface with dry characteristics offers an effective approach for preventing salt water infiltration (Yawei Yang et al. 2018a, b).

A wood-based device was prepared by coating a wood with hydrophobic laser-induced graphene. This layer prevented salt accumulation on the surface of the photoabsorber (Huang et al. 2020). Song et al. used a strategy for continuous interfacial solar steam generation by preparing a double-layer wood-based evaporator. The wood substrate was delignified to improve wetting and thermal properties. The delignification of wood provided a more hydrophilic substrate and larger channels, allowing enhanced water transportation and less salt accumulation (Song et al. 2021).

A photoabsorber was also prepared by coating a wood surface with a thin layer of Fe_3O_4 as a light absorber and polyvinyl alcohol to improve affinity between the wood and Fe_3O_4. The device's surface was hydrophobic with a contact angle of 132°, whereas the lowest surface of a wood substrate was superhydrophilic with a contact angle of 6°. This asymmetric wettability further promoted solar to thermal conversion and enabled a continuous interfacial solar steam generation in a 3.5 wt% NaCl solution. The evaporation flux of 1.3 kg m^{-2} h^{-1} and efficiency of 73% were achieved under 1 sun by this photoabsorber (Song et al. 2021). The device also presented a good antifouling property due to the following reasons:

1. Salts cannot deposit on the hydrophobic layer.
2. The rapid water uptake enhances the redissolution of salts into the water.

A solar evaporator was fabricated by a hydrophobic wood by immersing it in polydimethylsiloxane and hydrophobic SiO_2 nanoparticles and a hydrophilic solar absorber of carbon black/polyvinyl alcohol composite coated on a cotton. The solar evaporator could be suspended stably just underneath the water surface due to the surface tension force produced by the hydrophobic frame, enabling the confinement of a thin film of water on the photoabsorber for salt resistance and efficient utilization of energy. The suspending depth was kept unchanged in the brine with different salinity leading to achieve high evaporation fluxes of 1.45 and 1.35 kg m^{-2} h^{-1} in highly concentrated salt solutions of 15 and 20 wt% NaCl, respectively, under 1 sun. No salt accumulation was observed during the evaporation process (Y. Q. Luo et al. 2021a, b).

A double-layer photoabsorber was designed with a hydrophobic/hydrophilic structure for the interfacial solar steam generation of seawater consisting of alkaline earth metal-doped VO_2 nanoparticles as photothermal materials and poplar wood as a sustainable substrate. The upper layer of VO_2@alkaline earth metals with a hydrophobic character could prevent the salt accumulation on the surface and block the dissolved salts underneath itself. The hydrophilic bottom layer could pump the water upward. After desalination, the Na^+ concentration in the seawater reduced significantly (Aziznezhad et al. 2022).

2. The self-cleaning property caused by open microchannels is a phenomenon in which salt accumulated on the evaporative surface redissolves into bulk water via diffusion, resulting in the creation of a trade-off between salt deposited

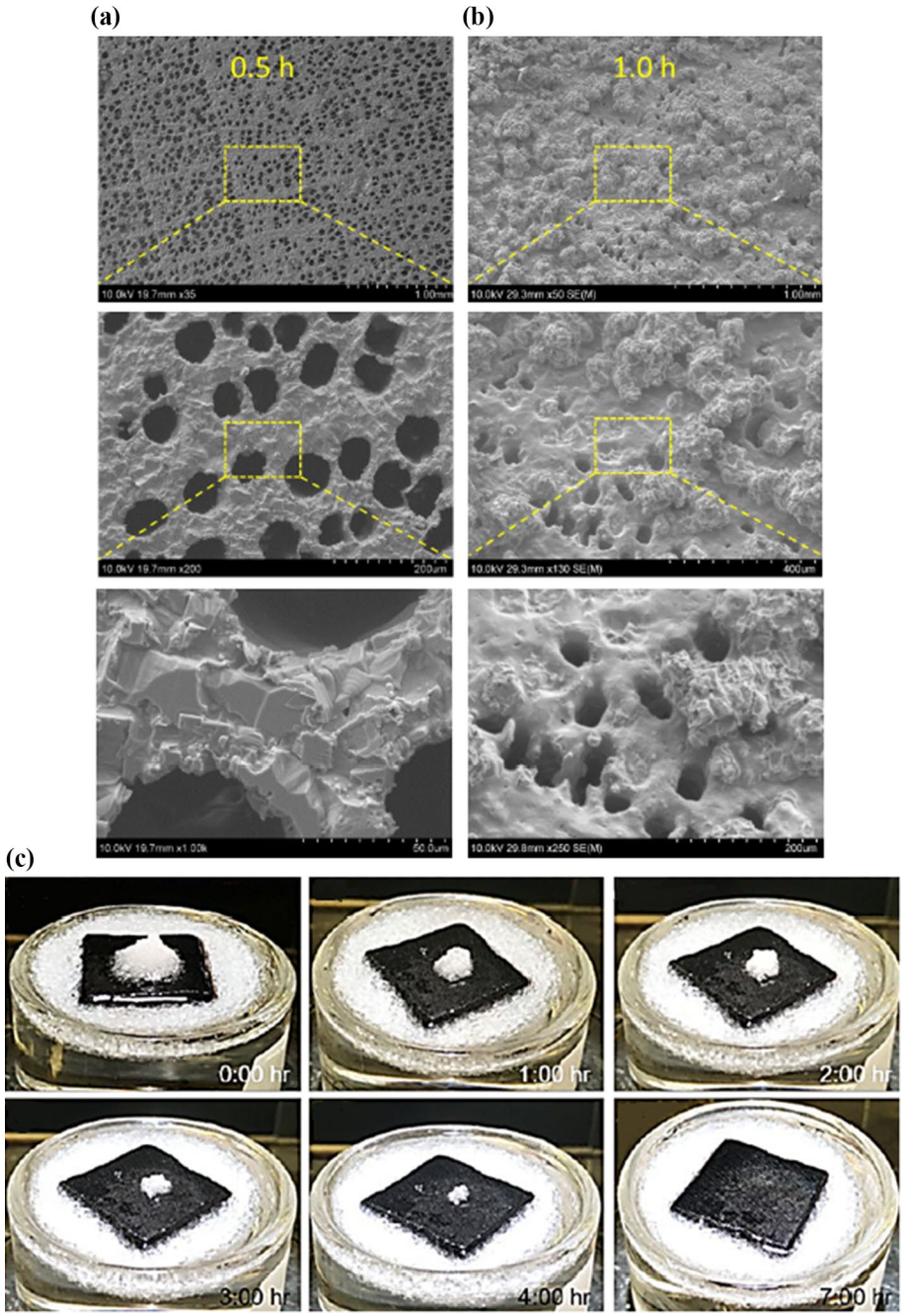

Fig. 9 Scanning electron microscopy images illustrating salt accumulation at the surface of conventional wood-based solar steam generation devices in 20 wt% NaCl for **a** 0.5 h and **b** 1 h under 1 sun. The small-sized microchannels (tracheids) with 12 μm in diameter were first blocked after 0.5 h. After 1-h desalination, severe salt deposit was observed at the photoabsorber's surface so that large-sized microchannels (vessels) with 50 μm in diameter are also blocked. In fact, due to low hydraulic conductivity, microchannels are not able to self-regenerate quickly resulting in salt blockage in the vessels and tracheids after a while. Reproduced with permission of Wiley from Kuang et al., (2019b). **c** Time-elapse snapshots show salt rejection from the surface of a self-cleaning photoabsorber (bimodal porous balsa wood) under 2 sun. After 7-h light illumination, all NaCl crystals put on the surface of bimodal porous balsa wood gradually dissolved back to the brine solution showing its excellent salt rejection capability. Owing to a big difference between concentration of the brine on the surface and the bulk brine, the salts also dissolve back into the bulk by diffusion and convection. Reproduced with permission of RSC from S. He et al. (2019a, b)

and dissolved (Kuang et al. 2019b; Wu et al. 2019a, b, c). This phenomenon is assigned to the difference in porosity and hydraulic conductivities of tracheids and vessels, leading to the exchange of salt between them via pits. As a result, solid NaCl placed on the top surface of wood-based solar steam generation devices (high salinity) gradually dissolves back to the bulk brine solution (low salinity) after a while, as shown in Fig. 9c (He et al. 2019a, b).

Zhu et al. revealed that open microstructures in the plasmonic wood photoabsorber exhibit the self-cleaning property. Microchannels with a large diameter inhibit salt-blocking properties so that the salts accumulated during the day diffused back into a bulk fluid at night (Zhu et al. 2018a, b). A photoabsorber was prepared by open microchannels, exhibiting excellent self-cleaning properties even after 6 h of continuous desalination under 1 sun in the salinity of 3.5 wt% (Huang et al. 2019).

A self-regenerating photoabsorber was also fabricated by drilling channels within a wood structure for long-term solar desalination. Compared with conventional solar evaporators (in which salt is deposited on the top surface after a short time), the surface of the prepared photoabsorber remained

without salt after a long period. This is because the salt is transferred fast to the bulk through drilled channels (Kuang et al. 2019b).

Yang et al. investigated the self-cleaning mechanism of the Ag-polydopamine@balsa wood by conducting the structure characterization of the photoabsorber. They observed that the surface of the Ag-polydopamine@balsa wood is mainly composed of vessel and tracheid channels with different porosities. The salt precipitated on the Ag-polydopamine@balsa wood surface dissolved via small and large microchannels into the seawater underneath, confirming that the Ag-polydopamine@balsa wood has an excellent self-cleaning capability (Yang et al. 2020).

Some holes with a diameter of 1.5 mm were drilled using a laser on a reduce graphene oxide/Ag/wood double-layer photoabsorber to improve the photoabsorber performance. The evaporation efficiency of the first cycle increased from 92.91% for wood/reduce graphene oxide/Ag to 122.06% for drilled wood-reduce graphene oxide/Ag under 3 sun. In addition, the evaporation performance of drilled photoabsorber did not change even after 11 cycles (Ebrahimi et al. 2022).

Scalable applications of wood-based solar steam generation devices

Due to sustainability, simple preparation, green, and cost-effectiveness, wood-based solar steam generation devices represent considerable potential for the following practical applications:

1. Solar desalination: efficient solar desalination results in a significant decrease of condensed water salinities meeting freshwater standards. High evaporation flux and efficiency in low solar intensities and high salinities, stability and durability, and antifouling properties for long-term applications are of great importance in wood-based solar steam generation devices (Kashyap and Ghasemi, 2020). State-of-the-art designs of the rational photoabsorbers have enhanced the evaporation efficiency of wood-based solar steam generation devices and provided their large-scale applications under 1 sun (Gao et al. 2018; Zhao et al. 2018a).

Tian et al. designed a rational sandwich photoabsorber, consisting of confined $CuCl_2$-carbon cells between two polyvinylidene fluoride membranes, which was placed on the wood surface (Fig. 10a). Owing to the efficient light harvesting of porous carbon cells, along with the excellent water transfer by the sandwich structure, the fabricated photoabsorber achieved the 1.87 kg m^{-2} h^{-1} evaporation flux at 1 sun. Moreover, the photoabsorber exhibited an excellent self-cleaning performance (Tian et al. 2020). A practical desalination device was designed made from paulownia wood coated with titanium carbide. The photoabsorber represented the evaporation flux of 1.465 kg m^{-2} h^{-1} under 1 sun (Ma et al. 2020).

Most of the wood-based solar steam generation devices are prepared by relatively expensive photothermal materials, such as Au and carbon nanotubes, or complicated preparation methods consuming high energy, such as high-temperature carbonization (Wang et al. 2019a, b, c). Hence, it is necessary to design low-cost photothermal materials by an energy-saving preparation process for use in wood-based devices that have potential for scalable and practical applications (Gao et al. 2019a, b; Wang et al. 2019a, b, c; Yu et al. 2019). For instance, the biomass-derived, catechol-containing compounds coordinated with metal cations have been used as efficient photothermal materials with cheap, green, and convenient preparation (Lei et al. 2016; Luo et al. 2019; Wu et al. 2017).

A natural phenolic substance coordinated with Fe^{3+} was introduced as a wood-based photoabsorber for real-world applications due to its cost-effective nature and high photothermal conversion efficiency under 1 sun (Gao et al. 2019a, b). A wood-based device was also prepared through the use of low-cost household candle soot in the absence of chemical reagents (Wang et al. 2019a, b, c). Polypyrrole-wood was also prepared through an environmentally friendly process and without any high temperature or carbonization treatment (Huang et al. 2019). Yu et al. synthesized carbonized wood ($1.84 per m^2) at an optimized thickness (2.2 cm), which is highly feasible for solar desalination applications at a large scale (Yu et al. 2019). A thermally stable wood-derived aerogel was designed via the delignification process and thermal treatment of wood which was cost efficient ($9.29 per kg) for practical applications (Meng et al. 2021).

2. Purification of the wastewater: the solar stills similar to water desalination are used for wastewater treatment such as dye degradation and heavy metal sorption (Brião et al. 2020; Deng et al. 2018; Higgins et al. 2018; Kiriarachchi et al. 2018; Kumar et al. 2021; Lopes et al. 2021; Peng and Guo, 2020; Soares et al. 2020; Yawei Yang et al. 2018a, b; Yuan et al. 2020; P. Zhang et al. 2018a, b). A mesoporous three-dimensional basswood decorated with Pd nanoparticles was used for efficient wastewater treatment, including a methylene blue solution. The plasmonic effect of Pd nanoparticles inside the wood channels caused Pd nanoparticles/wood to appear black. Three-dimensional Pd nanoparticles/wood exhibited a water treatment rate of 1×105 L m^{-2} h^{-1} and 99.8% methylene blue removal efficiency (Chen et al. 2017a, b, c).

A carbonized wood was also used as an evaporator for interfacial solar steam generation and a photocatalyst for methylene blue dye removal (Yu et al. 2019). After desalination, methylene blue was removed with 100% efficiency. Zhu et al. used carbonized daikon for the treatment of wastewater containing methyl orange dye. As illustrated in Fig. 10b,

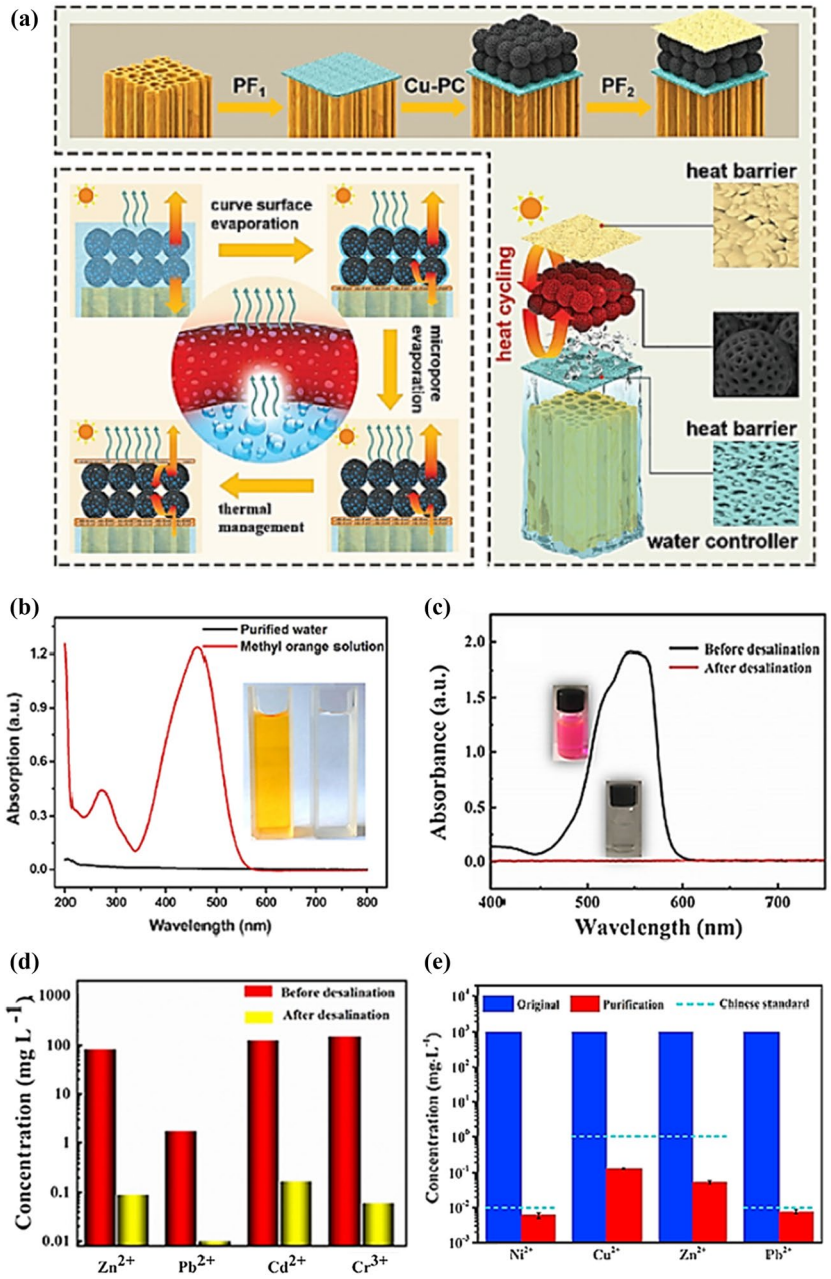

Fig. 10 **a** Fabrication and structure of the sandwich photothermal material coated wood and evaporation modes adjustment on different membrane structures. In this structure, $CuCl_2$-activated hierarchical porous carbon cells (Cu-PCs) are confined between two membranes of polyvinylidene fluoride (bottom and top layers denoted as PF_1 and PF_2, respectively). Due to the excellent performance of PF_1 in monitoring the water transfer, the water amount in the photothermal layer (Cu-PC) became controllable. Consequently, the decrease of water film formation around Cu-PC led to enhancement of Cu-PC performance in obtaining high evaporation rate. Reproduced with permission of Wiley from Tian et al. (2020). **b** The UV–vis spectrum of aqueous solution of **b** methyl orange and **c** rhodamine B before and after solar thermal purification (the inserts show the color of the solutions). The purified water was completely colorless and the dyes characteristic absorption peaks disappeared. These results imply dyes concentrations become very low due to solar desalination. Reproduced with permission of Elsevier from Zhu et al. (2019a, b, c) and Li et al., (2020). **d**, **e** Concentrations of heavy metal ions before and after desalination. After solar photothermal purification, the concentrations of all ions significantly reduced indicating great potential of wood-based photoabsorbers in water treatment applications. Reproduced with permission of Elsevier from Li et al. (2020) and Peng et al. (2021). **f** Photodegradation mechanism of reactive black 5 (RB5) dye by reduced graphene oxide (RGO) /graphitic carbon nitride ($g\text{-}C_3N_4$)/wood under solar irradiation. The electrostatically effective interface was created through reduced graphene oxide and $g\text{-}C_3N_4$ in the photoabsorber. Due to lower Fermi level of reduced graphene oxide than the conduction band of $g\text{-}C_3N_4$, photo-generated electrons (e^-) of $g\text{-}C_3N_4$ CB (with creating holes (h^+) in valance band) transported to the reduced graphene oxide surface. Storage of electron by reduced graphene oxide as an effective scaffold decreased the recombination rate of $e^- - h^+$ pairs. Superoxide radicals ($O_2^{-\circ}$) and hydroxyl radicals (OH°) were generated by charge carriers which are responsible for RB5 degradation. Reproduced with permission of Elsevier from Karimi-Nazarabad et al. (2021)

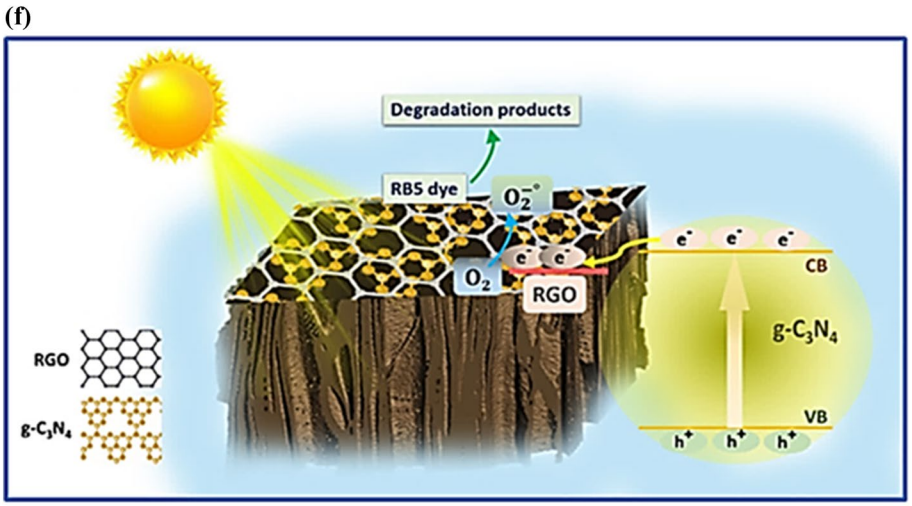

Fig. 10 (continued)

they removed dye completely after desalination (Zhu et al. 2019a, b, c). A wastewater containing Zn^{2+}, Cd^{2+}, Pb^{2+}, Cr^{3+} heavy metal ions was purified and rhodamine B dye in the presence of WO_{3-x}-wood under solar illumination (Fig. 10c and d) (Li et al. 2020).

A candle soot-wood was also used for the interfacial solar steam generation of saline water containing heavy metal. The concentration of each metal ion was below the standard limit after desalination (Fig. 10e) (Peng et al. 2021). A chemically treated carbonized wood was used as a solar absorber and heavy metal ion adsorber. Through this device, a higher rate of water evaporation and heavy metal ion removal was attained with respect to carbonized wood. Pb^{2+} sorption capacity was also enhanced over 225% as solar intensity increased to 3 sun (Hou et al. 2021).

A reduce graphene oxide/graphitic carbon nitride/wood was utilized as a multifunctional device for seawater interfacial solar steam generation, photodegradation of reactive black 5 dye, and Pb (II) sorption from aqueous solutions. The dye was completely degraded under the sunlight, displaying the synergistic effect of graphitic carbon nitride and reduce graphene oxide in improving charge carriers' separation. The superoxide radicals were mainly responsible for the dye photodegradation (Fig. 10f). In addition, reduce graphene oxide/graphitic carbon nitride/wood could completely adsorb Pb (II) ions within less than 5 min (Karimi-Nazarabad et al. 2021).

3. Oil/water separation: in addition to solar-based applications, wood-based materials could also be used in oil/water separation (Fang et al. 2021). A paper filter modified by nanofibrillated cellulose hydrogel separated an emulsion of hexane/water with the 89.6 L m^{-2} h^{-1} separation flux (Rohrbach et al. 2014). A toluene/water emulsion was separated by a cellulose sponge with 99.9% efficiency (Wang et al. 2015). A polyvinyl alcohol crosslinked filter paper separated mixtures of hexane/water with 99.9% efficiency and high stability after 20 cycles in harsh conditions (Fan et al. 2015).

A sponge of delignified wood modified by methyltrimethoxysilane had a 41 g g^{-1} sorption capacity of chloroform (Song et al. 2019). A composite of epoxy and delignified wood had high-absorption capacities for several oils (Fu et al. 2018a, b). A membrane consisting of layered double hydroxide and filter paper separated a mixture of chloroform/water with the 4968 L m^{-2} h^{-1} separation rate (Yue et al. 2017). A delignified basswood coated by cellulose exhibited efficient oil/water separation ability due to the chemical structure of cellulose. The delignified basswood was able to separate several mixtures of oil/water with a flux of 41,558 L m^{-2} h^{-1} (Wu et al. 2019a, b, c).

A wood carbon modified by hexamethyldisilazane-silicon dioxide had a 1.6 L m^{-2} oil absorption rate within 30 s under 1 sun (Kuang et al. 2019a). A composite of delignified wood aerogel and polydimethylsiloxane separated mixtures of trichloromethane/water with an 99.5% efficiency (Wang et al. 2019a, b, c). A filter paper/polyvinyl alcohol membrane separated various oil/water emulsions with a separation flux and efficiency greater than 37 L m^{-2} h^{-1} and 98%, respectively (Xu et al. 2019).

A superhydrophobic carbon nanotubes/wood aerogel was fabricated for efficient oil recovery. The aerogel reserved the hierarchical structure of natural wood through the selective removal of lignin and hemicellulose, followed by a freeze-drying process (Zhu et al. 2019a, b, c). A sulfonated nanofibrillated cellulose aerogel separated a mixture of kerosene/water with a 360 L m^{-2} h^{-1} flux. The aerogel showed high stability after 20 cycles (Sun et al. 2017).

Table 3 Cost-effective performance of wood-based solar steam generation devices in comparison with other photoabsorbers

Photoabsorber	Evaporation flux (kg m^{-2} h^{-1})	ε (g h^{-1} $\$^{-1}$)	References
Arched bamboo charcoal	1.34	1340.00	Li et al. (2019a, b, c)
[a]HT-wood	2.89	1333.00	Ghafurian et al. (2020b)
[b]LT-wood	2.52	1052.00	Ghafurian et al. (2020b)
[c]LT-HT-wood	2.99	1041.00	Ghafurian et al. (2020b)
Carbonized wood	1.21	657.30	Yu et al. (2019)
[d]Au-HT-wood	4.02	285.40	Ghafurian et al. (2020b)
Au-wood	3.54	260.20	Ghafurian et al. (2020b)
Reduce graphene oxide/Ag-wood	5.99	113.66	Ebrahimi et al. (2022)
FeNi/reduce graphene oxide double-layer wood	4.77	51.37	Mehrkhah et al. (2021a)
Reduce graphene oxide/FeNi composite -wood	4.19	41.9	Mehrkhah et al. (2021b)
Reduce graphene oxide/graphitic carbon nitride/wood	5.20	13.61	Karimi-Nazarabad et al. (2021)
[d]HTW5F5	3.32	1.12	Ghafurian et al. (2020c)
[e]FePdW5F5	3.88	0.53	Ghafurian et al. (2020c)
[f]AuW5F5	4.00	0.28	Ghafurian et al. (2020c)
Pd-wood	3.20	0.05	M. Zhu et al. (2018a, b)
Polypyrrole-wood	3.80	0.11	Huang et al. (2019)
Al nanoparticles/anodic aluminum oxide membrane	1.40	0.05	Zhou et al. (2016)
Graphite-carbon foam	1.20	0.14	Ghasemi et al. (2014)
Au-TiO_2 membrane	2.70	0.48	Huang et al. (2017)
Au deposited nanoporous template	4.00	0.24	Zhou et al. (2016)
Copper prototype	2.88	1.01	Morciano et al. (2017)
Cermet-coated copper sheet/polystyrene foam	0.50	8.26	Ni et al. (2016)
Flexible thin-film black gold membrane	0.60	0.01	Bae et al. (2015)
Graphene oxide/carbon nanotube/nanofibrillated cellulose	1.10	10.40	Li et al. (2017b)
Graphene oxide film/cellulose/polystyrene foam	1.40	65.50	Li et al. (2016a, b)
Hierarchical graphene foam	1.50	3.50	Ren et al. (2017)
Vertically aligned graphene sheets	1.60	100.05	Zhang et al. (2017)
Cu_2SnSe_3 nanosphere /filter membrane	1.65	40.26	Yang et al. (2018a, b)
Plant cellulose wrapped cotton cores	1.70	10.30	Li et al. (2018a)
NiFe-layered double hydroxide/$CuOH)_2$	1.65	10.28	Luo et al. (2021a, b)
Quartz glass fibrous filter membrane/metal nitrate mixture	2.10	4.50	Shi et al. (2018)
Polyvinyl alcohol/polypyrrole gel	3.25	25.40	Zhao et al. (2018b)
Sponge-like hydrogel	3.00	9.32	Guo et al. (2019)
Konjac glucomannan/iron-based metal–organic/polyvinyl alcohol	3.20	214.16	Guo et al. (2020)
Cellulose-based fabric/polystyrene	0.70	233.02	Ni et al. (2018)
Multilayer polypyrrole nanosheets	1.30	60.25	Wang et al. (2019a, b, c)

[a]Carbonized wood

[b]Laser treatment wood

[c]Laser treatment wood followed by the hot plate carbonization

[d]Carbonized wood on polystyrene foam with 5 mm diameter

[e]Fe/Pd coated on wood and polystyrene foam with 5 mm diameter

[f]Au coated on wood and polystyrene foam with 5 mm diameter

Cost-effective performance of wood-based solar steam generation devices

The scalability and cost-effectiveness of a solar evaporator are also very important in practical applications. The main drawbacks in the use of the current photoabsorbers, including high-cost, complex preparation, and the need for high sun illumination result in employing additional optical focusing devices that largely limit practical implementations of the photoabsorbers. Hence, the design of cost-effective

photothermal materials with superior performance, an easy manufacturing process, and high efficiency under 1 sun is of great importance.

For reaching this goal, the economic performance of wood-based solar steam generation devices in terms of the ratio of the evaporation rate to the preparation cost should be computed (Eqs. 35 and 36) (Mehrkhah et al. 2021b; Wang et al. 2022a):

$$\frac{SSG\ rate}{Cost}\left(cm^3h^{-1}/\$\right) = \frac{\dot{m} \times A}{Cost \times \rho_w} \tag{35}$$

where ρ_w is the density of water. A is the photoabsorber surface area. $\dot{m}$ is the water evaporation flux.

$$\varepsilon\left(kg/h\$\right) = \frac{\dot{m}}{c} \tag{36}$$

where ε stands for the cost-effective performance of the photoabsorber and c denotes the preparation cost of 1 m^2 of the evaporator ($\$\ m^{-2}$). For this purpose, the water evaporation flux and production cost of wood-based solar steam generation devices with a certain surface area, A, are calculated. For instance, according to Eq. 35, the ratio of preparation cost to interfacial solar steam generation rate for a laboratory-scaled reduce graphene oxide/ graphitic carbon nitride/ wood photoabsorber with $\dot{m}$, A, and the preparation cost of 5.20 g cm^{-2} h^{-1}, 12.56 cm^2, and 0.484 $, respectively, was calculated as 0.07 $\$\ cm^{-3}$ h (Karimi-Nazarabad et al. 2021). According to Eq. 36, ε is calculated as 332 g h^{-1} $\$^{-1}$ for a porous hydrogel sponge photoabsorber with the evaporation rate of 2.8 kg m^{-2} h^{-1} and preparation cost of 0.92 $\$\ m^{-2}$ (Wang et al. 2022a, b). Table 3 compares the economic performance of wood-based devices with other photoabsorbers. As shown in Table 3, wood-based solar steam generation devices show more cost-effective performance in interfacial solar steam generation with respect to other photoabsorbers. Although some synthetic substrates, such as polymeric foams, seem to be more cost effective, utilization of such nonbiodegradable substrates has a negative impact on the environment. Therefore, wood-based devices are the most appealing solar evaporators owing to their low cost, biodegradability, abundance, ease of use, and natural, three-dimensional interconnected porous structure (Wang et al. 2022a).

Conclusion

In this review, wood properties were provided which have several promising applications in a wide range of technologies such as interfacial solar steam generation. Wood-based solar steam generation devices have received great attention in interfacial solar steam generation because of their high evaporation efficiency. The performance of wood-based solar steam generation devices is affected by several factors, including the heat loss, photoabsorber geometry, wood texture, and several environmental conditions such as water depth, relative humidity, and water salinity.

In recent years, remarkable developments in wood-based solar steam generation devices from the design of different photothermal materials to treatment of wood substrates greatly motivate this research area. However, despite the encouraging progress in wood-based solar steam generation devices, there are several crucial challenges in their large-scale applications which should be taken into account:

1. Long-term chemical and physical stabilities of wood-based solar steam generation devices are need to be considered in harsh conditions.
2. Scalability and economic-based analyses are two important considerations. Therefore, it is desirable to develop wood-based solar steam generation devices with scalable and low-cost processes.
3. Salt-blocking and mildew-resistant issues are inevitable in wood-based solar steam generation devices. Salt- and mildew-blocking not only decrease the solar absorption as a result from increase reflection by the deposit layer, but they also reduce water transportation abilities due to the blocking of the water transport routes. To date, several solutions have been suggested for addressing this challenge, including using metal and metal oxide nanoparticles, wood-based aerogel, graphene, hydrophobic membrane, and wood with open microchannels.

Acknowledgements This research was supported by Incheon National University in 2021.

Funding The authors have not disclosed any funding.

Declarations

Conflict of interest The authors declare that they have no known competing financial interests or personal relationships that could have appeared to influence the work reported in this paper.

References

Akhavan O, Ghaderi E (2010) Toxicity of graphene and graphene oxide nanowalls against bacteria. ACS Nano 4:5731–5736. https://doi.org/10.1021/nn101390x

Akhlamadi G, Goharshadi EK (2021) Sustainable and superhydrophobic cellulose nanocrystal-based aerogel derived from waste tissue paper as a sorbent for efficient oil/water separation. Process Saf Environ Prot 154:155–167. https://doi.org/10.1016/j.psep.2021.08.009

Amjad M, Jin H, Du X, Wen D (2018) Experimental photothermal performance of nanofluids under concentrated solar flux. Sol

Energy Mater Sol Cells 182:255–262. https://doi.org/10.1016/j.solmat.2018.03.044
Arunkumar T, Murugesan D, Raj K, Denkenberger D, Viswanathan C, Rufuss DDW, Velraj R (2019) Effect of nano-coated CuO absorbers with PVA sponges in solar water desalting system. Appl Therm Eng 148:1416–1424. https://doi.org/10.1016/j.applthermaleng.2018.10.129
Awad FS, Kiriarachchi HD, Abouzeid KM, Özgür Ü, El-Shall MS (2018) Plasmonic graphene polyurethane nanocomposites for efficient solar water desalination. ACS Appl Energy Mater 1:976–985. https://doi.org/10.1021/acsaem.8b00109
Aziznezhad M, Goharshadi E, Namayandeh-Jorabchi M (2020) Surfactant-mediated prepared VO2 (M) nanoparticles for efficient solar steam generation. Sol Energy Mater Sol Cells. https://doi.org/10.1016/j.solmat.2020.110515
Aziznezhad M, Goharshadi EK, Mehrkhah R, Ghafurian MM (2022) Alkaline earth metals doped VO2 nanoparticles for enhanced interfacial solar steam generation. Mater Res Bull 149:111705. https://doi.org/10.1016/j.materresbull.2021.111705
Bae K, Kang G, Cho SK, Park W, Kim K, Padilla WJ (2015) Flexible thin-film black gold membranes with ultrabroadband plasmonic nanofocusing for efficient solar vapour generation. Nat Commun. https://doi.org/10.1038/ncomms10103
Bakthavatchalam B, Habib K, Saidur R, Saha BB, Irshad K (2020) Comprehensive study on nanofluid and ionanofluid for heat transfer enhancement: a review on current and future perspective. J Mol Liq 305:112787. https://doi.org/10.1016/j.molliq.2020.112787
Brião GDV, de Andrade JR, da Silva MGC, Vieira MGA (2020) 2020 Removal of toxic metals from water using chitosan-based magnetic adsorbents: a review. Environ Chem Lett 18(1145):1168. https://doi.org/10.1007/s10311-020-01003-y
Cao P, Zhao L, Zhang J, Zhang L, Yuan P, Zhang Y, Li Q (2021) Gradient heating effect modulated by hydrophobic/hydrophilic carbon nanotube network structures for ultrafast solar steam generation. ACS Appl Mater Interfaces 13:19109–19116
Carrillo CA, Nypelö T, Rojas OJ (2016) Double emulsions for the compatibilization of hydrophilic nanocellulose with non-polar polymers and validation in the synthesis of composite fibers. Soft Matter 12:2721–2728. https://doi.org/10.1039/C5SM02578H
Chen C, Li Y, Song J, Yang Z, Kuang Y, Hitz E, Jia C, Gong A, Jiang F, Zhu JY, Yang B, Xie J, Hu L (2017a) Highly flexible and efficient solar steam generation device. Adv Mater 29:1701756. https://doi.org/10.1002/adma.201701756
Chen C, Zhang Y, Li Y, Dai J, Song J, Yao Y, Gong Y, Kierzewski I, Xie J, Hu L (2017b) All-wood{,} low tortuosity{,} aqueous{,} biodegradable supercapacitors with ultra-high capacitance. Energy Environ Sci 10:538–545. https://doi.org/10.1039/C6EE03716J
Chen F, Gong AS, Zhu M, Chen G, Lacey SD, Jiang F, Li Y, Wang Y, Dai J, Yao Y, Song J, Liu B, Fu K, Das S, Hu L (2017c) Mesoporous, three-dimensional wood membrane decorated with nanoparticles for highly efficient water treatment. ACS Nano 11:4275–4282. https://doi.org/10.1021/acsnano.7b01350
Chen W, Yu H, Lee SY, Wei T, Li J, Fan Z (2018) Nanocellulose: a promising nanomaterial for advanced electrochemical energy storage. Chem Soc Rev 47:2837–2872. https://doi.org/10.1039/c7cs00790f
Chen C, Kuang Y, Hu L (2019a) Challenges and opportunities for solar evaporation. Joule 3:683–718. https://doi.org/10.1016/j.joule.2018.12.023
Chen Z, Dang B, Luo X, Li W, Li J, Yu H, Liu S, Li S (2019b) Deep eutectic solvent-assisted in situ wood delignification: a promising strategy to enhance the efficiency of wood-based solar steam generation devices. ACS Appl Mater Interfaces 11:26032–26037. https://doi.org/10.1021/acsami.9b08244
Chen T, Wu Z, Liu Z, Aladejana JT, Wang X, Niu M, Xie Y (2020) Hierarchical porous aluminophosphate-treated wood for high-efficiency solar steam generation. ACS Appl Mater Interfaces 12:19511–19518. https://doi.org/10.1021/acsami.0c01815
Chen M, Lin X, Zeng C, He Q (2021) Poly (p-phenylene benzobisoxazole) nanofiber/reduced graphene oxide composite aerogels toward high-efficiency solar steam generation. Colloids Surf A Physicochem Eng Asp 612:125997
Colangelo G, Favale E, Miglietta P, Milanese M, de Risi A (2016) Thermal conductivity, viscosity and stability of Al2O3-diathermic oil nanofluids for solar energy systems. Energy 95:124–136. https://doi.org/10.1016/j.energy.2015.11.032
Cui L, Zhang P, Xiao Y, Liang Y, Liang H, Cheng Z, Qu L (2018) High rate production of clean water based on the combined photo-electro-thermal effect of graphene architecture. Adv Mater. https://doi.org/10.1002/adma.201706805
Darling SB (2018) Perspective: Interfacial materials at the interface of energy and water. J Appl Phys 124:030901. https://doi.org/10.1063/1.5040110
Deng Z, Zhou J, Miao L, Liu C, Peng Y, Sun L, Tanemura S (2017) The emergence of solar thermal utilization: solar-driven steam generation. J Mater Chem A 5:7691–7709. https://doi.org/10.1039/c7ta01361b
Deng Z, Liu P-F, Zhou J, Miao L, Peng Y, Su H, Wang P, Wang X, Cao W, Jiang F, Sun L, Tanemura S (2018) A novel ink-stained paper for solar heavy metal treatment and desalination. Sol RRL 2:1800073. https://doi.org/10.1002/solr.201800073
Ding D, Wu H, He X, Yang F, Gao C, Yin Y, Ding S (2021) A metal nanoparticle assembly with broadband absorption and suppressed thermal radiation for enhanced solar steam generation. J Mater Chem A 9:11241–11247
Donaldson LA, Cairns M, Hill SJ (2018) Comparison of micropore distribution in cell walls of softwood and hardwood xylem. Plant Physiol 178:1142–1153
Ebrahimi A, Goharshadi EK, Mohammadi M (2022) Reduced graphene oxide/silver/wood as a salt-resistant photoabsorber in solar steam generation and a strong antibacterial agent. Mater Chem Phys 275:125258. https://doi.org/10.1016/j.matchemphys.2021.125258
Elsheikh AH, Sharshir SW, Ahmed Ali MK, Shaibo J, Edreis EMA, Abdelhamid T, Du C, Haiou Z (2019) Thin film technology for solar steam generation: a new dawn. Sol Energy 177:561–575. https://doi.org/10.1016/j.solener.2018.11.058
Ercin AE, Hoekstra AY (2014) Water footprint scenarios for 2050: a global analysis. Environ Int 64:71–82. https://doi.org/10.1016/j.envint.2013.11.019
Fan J, Song Y, Wang S, Meng J, Yang G, Guo X, Feng L, Jiang L (2015) Directly coating hydrogel on filter paper for effective oil–water separation in highly acidic, alkaline, and salty environment. Adv Funct Mater 25:5368–5375
Fang M, Chen J-H, Xu X-L, Yang P-H, Hildebrand HF (2006) Antibacterial activities of inorganic agents on six bacteria associated with oral infections by two susceptibility tests. Int J Antimicrob Agents 27:513–517
Fang J, Liu Q, Zhang W, Gu J, Su Y, Su H, Guo C, Zhang D (2017) Ag/diatomite for highly efficient solar vapor generation under one-sun irradiation. J Mater Chem A 5:17817–17821. https://doi.org/10.1039/c7ta05976k
Fang J, Liu J, Gu J, Liu Q, Zhang W, Su H, Zhang D (2018) Hierarchical porous carbonized lotus seedpods for highly efficient solar steam generation. Chem Mater 30:6217–6221. https://doi.org/10.1021/acs.chemmater.8b01702
Fang Y, Jing C, Li G, Ling S, Wang Z, Lu P, Li Q, Dai C, Gao S, Chen B, Bai L, Zhang H, Liu T, Wang Q, Li J, Yu H, Liu S, Chen W (2021) Wood-derived systems for sustainable oil/water

separation. Adv Sustain Syst 5:1–13. https://doi.org/10.1002/adsu.202100039
Finnerty C, Zhang L, Sedlak DL, Nelson KL, Mi B (2017) Synthetic graphene oxide leaf for solar desalination with zero liquid discharge. Environ Sci Technol 51:11701–11709. https://doi.org/10.1021/acs.est.7b03040
Fu Q, Yan M, Jungstedt E, Yang X, Li Y, Berglund LA (2018a) Transparent plywood as a load-bearing and luminescent biocomposite. Compos Sci Technol 164:296–303
Fu QL, Ansari F, Zhou Q, Berglund LA (2018b) Wood nanotechnology for strong, mesoporous, and hydrophobic biocomposites for selective separation of oil/water mixtures. ACS Nano 12(3):2222–2230
Gao X, Lan H, Li S, Lu X, Zeng M, Gao X, Wang Q, Zhou G, Liu J-M, Naughton MJ, Kempa K, Gao J (2018) Artificial mushroom sponge structure for highly efficient and inexpensive cold-water steam generation. Glob Challenges 2:1800035. https://doi.org/10.1002/gch2.201800035
Gao H, Yang M, Dang B, Luo X, Liu S, Li S, Chen Z, Li J (2019a) Natural phenolic compound-iron complexes: sustainable solar absorbers for wood-based solar steam generation devices. RSC Adv 10:1152–1158. https://doi.org/10.1039/c9ra08235b
Gao M, Zhu L, Peh CK, Ho GW (2019b) Solar absorber material and system designs for photothermal water vaporization towards clean water and energy production. Energy Environ Sci 12:841–864. https://doi.org/10.1039/c8ee01146j
Ghafurian MM, Akbari Z, Niazmand H, Mehrkhah R, Wongwises S, Mahian O (2020a) Effect of sonication time on the evaporation rate of seawater containing a nanocomposite. Ultrason Sonochem 61:104817. https://doi.org/10.1016/j.ultsonch.2019.104817
Ghafurian MM, Niazmand H, Ebrahimnia-Bajestan E, Taylor RA (2020b) Wood surface treatment techniques for enhanced solar steam generation. Renew Energy 146:2308–2315. https://doi.org/10.1016/j.renene.2019.08.036
Ghafurian MM, Niazmand H, Goharshadi EK, Zahmatkesh BB, Moallemi AE, Mehrkhah R, Mahian O (2020c) Enhanced solar desalination by delignified wood coated with bimetallic Fe/Pd nanoparticles. Desalination 493:114657. https://doi.org/10.1016/j.desal.2020.114657
Ghafurian MM, Dastjerd FT, Afsharian A, Esfahani FR, Niazmand H, Behzadnia H, Wongwises S, Mahian O (2021) Low-cost zinc-oxide nanoparticles for solar-powered steam production: superficial and volumetric approaches. J Clean Prod 280:124261. https://doi.org/10.1016/j.jclepro.2020.124261
Ghasemi H, Ni G, Marconnet AM, Loomis J, Yerci S, Miljkovic N, Chen G (2014) Solar steam generation by heat localization. Nat Commun 5:1–7. https://doi.org/10.1038/ncomms5449
Ghim D, Jiang Q, Cao SS, Singamaneni S, Jun YS (2018) Mechanically interlocked 1T/2H phases of MoS2 nanosheets for solar thermal water purification. Nano Energy 53:949–957. https://doi.org/10.1016/j.nanoen.2018.09.038
Gibson LJ (2012) The hierarchical structure and mechanics of plant materials. J R Soc Interface 9:2749–2766. https://doi.org/10.1098/rsif.2012.0341
Goharshadi EK, Abareshi M, Mehrkhah R, Samiee S, Moosavi M, Youssefi A, Nancarrow P (2011) Preparation, structural characterization, semiconductor and photoluminescent properties of zinc oxide nanoparticles in a phosphonium-based ionic liquid. Mater Sci Semicond Process. https://doi.org/10.1016/j.mssp.2011.01.011
Goharshadi EK, Sajjadi SH, Mehrkhah R, Nancarrow P (2012) Sonochemical synthesis and measurement of optical properties of zinc sulfide quantum dots. Chem Eng J 209:113–117
Goharshadi EK, Mehrkhah R, Nancarrow P (2013b) Synthesis, characterization, and measurement of structural, optical, and phtotoluminescent properties of zinc sulfide quantum dots. Mater Sci Semicond Process 16:356–362. https://doi.org/10.1016/j.mssp.2012.09.012
Goharshadi K, Sajjadi SA, Goharshadi EK, Mehrkhah R (2022) Highly efficient plasmonic wood/Ag/Pd photoabsorber in interfacial solar steam generation. Mater Res Bull. https://doi.org/10.1016/j.materresbull.2022.111916
Goharshadi EK, Ahmadzadeh H, Samiee S, Hadadian M, (2013a). Nanofluids for heat transfer enhancement-a review.
Gong B, Yang H, Wu S, Tian Y, Guo X (2021) Multifunctional solar bamboo straw : multiscale 3D membrane for self-sustained solar-thermal water desalination and puri fi cation and thermoelectric waste heat recovery and storage. Carbon NY 171:359–367. https://doi.org/10.1016/j.carbon.2020.09.033
Gu X, Xu Z, Gu L, Xu H, Han F, Chen B, Pan X (2021) Preparation and antibacterial properties of gold nanoparticles: a review. Environ Chem Lett 19:167–187. https://doi.org/10.1007/s10311-020-01071-0
Guan Q-F, Han Z-M, Ling Z-C, Yang H-B, Yu S-H (2020) Sustainable wood-based hierarchical solar steam generator: a biomimetic design with reduced vaporization enthalpy of water. Nano Lett 20:5699–5704
Guo D, Yang X (2019) Highly efficient solar steam generation of low cost TiN/bio-carbon foam. Sci China Mater 62:711–718
Guo Y, Zhou X, Zhao F, Bae J, Rosenberger B, Yu G (2019) Synergistic energy nanoconfinement and water activation in hydrogels for efficient solar water desalination. ACS Nano 13:7913–7919. https://doi.org/10.1021/acsnano.9b02301
Guo Y, Lu H, Zhao F, Zhou X, Shi W, Yu G (2020) Biomass-derived hybrid hydrogel evaporators for cost-effective solar water purification. Adv Mater 32:1–8. https://doi.org/10.1002/adma.201907061
Hajatzadeh Pordanjani A, Aghakhani S, Afrand M, Mahmoudi B, Mahian O, Wongwises S (2019) An updated review on application of nanofluids in heat exchangers for saving energy. Energy Convers Manag 198:111886. https://doi.org/10.1016/j.enconman.2019.111886
Hao W, Wu R, Zhang R, Ha Y, Chen Z, Wang L, Yang Y, Ma X, Sun D, Fang F, Guo Y (2018) Electroless plating of highly efficient bifunctional boride-based electrodes toward practical overall water splitting. Adv Energy Mater 8:1801372. https://doi.org/10.1002/aenm.201801372
Hassan H, Yousef MS (2021) An assessment of energy, exergy and CO2 emissions of a solar desalination system under hot climate conditions. Process Saf Environ Prot 145:157–171. https://doi.org/10.1016/j.psep.2020.07.043
He S, Chen C, Kuang Y, Mi R, Liu Y, Pei Y, Kong W, Gan W, Xie H, Hitz E, Jia C, Chen X, Gong A, Liao J, Li J, Ren ZJ, Yang B, Das S, Hu L (2019a) Nature-inspired salt resistant bimodal porous solar evaporator for efficient and stable water desalination. Energy Environ Sci 12:1558–1567. https://doi.org/10.1039/c9ee00945k
He Y, Li H, Guo X, Zheng R (2019b) Delignified wood-based highly efficient solar steam generation device via promoting both water transportation and evaporation. BioResources 14:3758–3767. https://doi.org/10.15376/biores.14.2.3758-3767
He F, Han M, Zhang J, Wang Z, Wu X, Zhou Y, Jiang L, Peng S, Li Y (2020) A simple, mild and versatile method for preparation of photothermal woods toward highly efficient solar steam generation. Nano Energy 71:104650. https://doi.org/10.1016/j.nanoen.2020.104650
Higgins MW, Shakeel Rahmaan AR, Devarapalli RR, Shelke MV, Jha N (2018) Carbon fabric based solar steam generation for waste water treatment. Sol Energy 159:800–810. https://doi.org/10.1016/j.solener.2017.11.055

Hou Q, Xue C, Li N, Wang H, Chang Q, Liu H, Yang J, Hu S (2019) Self-assembly carbon dots for powerful solar water evaporation. Carbon NY 149:556–563. https://doi.org/10.1016/j.carbon.2019.04.083

Hou Q, Zhou H, Zhang W, Chang Q, Yang J, Xue C, Hu S (2021) Boosting adsorption of heavy metal ions in wastewater through solar-driven interfacial evaporation of chemically-treated carbonized wood. Sci Total Environ 759:144317. https://doi.org/10.1016/j.scitotenv.2020.144317

Hu X, Xu W, Zhou L, Tan Y, Wang Y, Zhu S, Zhu J (2017) Tailoring graphene oxide-based aerogels for efficient solar steam generation under one sun. Adv Mater. https://doi.org/10.1002/adma.201604031

Huang J, He Y, Chen M, Jiang B, Huang Y (2017) Solar evaporation enhancement by a compound film based on Au@TiO2 core–shell nanoparticles. Sol Energy 155:1225–1232. https://doi.org/10.1016/j.solener.2017.07.070

Huang W, Hu G, Tian C, Wang X, Tu J, Cao Y, Zhang K (2019) Nature-inspired salt resistant polypyrrole–wood for highly efficient solar steam generation. Sustain Energy Fuels 3:3000–3008. https://doi.org/10.1039/C9SE00163H

Huang L, Ling L, Su J, Song Y, Wang Z, Tang BZ, Westerhoff P, Ye R (2020) Laser-engineered graphene on wood enables efficient antibacterial, anti-salt-fouling, and lipophilic-matter-rejection solar evaporation. ACS Appl Mater Interfaces 12:51864–51872. https://doi.org/10.1021/acsami.0c16596

Ibrahim I, Seo DH, McDonagh AM, Shon HK, Tijing L (2020) Semiconductor photothermal materials enabling efficient solar steam generation toward desalination and wastewater treatment. Desalination 500:114853

Irani M, Ghafurian MM, Khorasani MM, Mehrkhah R, Mahian O (2021) A comparative study of the effect of phase change material (paraffin wax) on volumetric and surface direct solar steam generation. J Taiwan Inst Chem Eng 128:253–260. https://doi.org/10.1016/j.jtice.2021.07.046

Jalal R, Goharshadi EK, Abareshi M, Moosavi M, Yousefi A, Nancarrow P (2010) ZnO nanofluids: green synthesis, characterization, and antibacterial activity. Mater Chem Phys 121:198–201

Jang H, Choi J, Lee H, Jeon S (2020) Corrugated wood fabricated using laser-induced graphitization for salt-resistant solar steam generation. ACS Appl Mater Interfaces 12:30320–30327. https://doi.org/10.1021/acsami.0c05138

Jia C, Li T, Chen C, Dai J, Kierzewski IM, Song J, Li Y, Yang C, Wang C, Hu L (2017a) Scalable, anisotropic transparent paper directly from wood for light management in solar cells. Nano Energy 36:366–373

Jia C, Li Y, Yang Z, Chen G, Yao Y, Jiang F, Kuang Y, Pastel G, Xie H, Yang B, Das S, Hu L (2017b) Rich mesostructures derived from natural woods for solar steam generation. Joule 1:588–599. https://doi.org/10.1016/j.joule.2017.09.011

Jilani A, Othman MHD, Ansari MO, Hussain SZ, Ismail AF, Khan IU, Inamuddin, (2018) Graphene and its derivatives: synthesis, modifications, and applications in wastewater treatment. Environ Chem Lett 16:1301–1323. https://doi.org/10.1007/s10311-018-0755-2

Jin H, Lin G, Bai L, Zeiny A, Wen D (2016) Steam generation in a nanoparticle-based solar receiver. Nano Energy 28:397–406. https://doi.org/10.1016/j.nanoen.2016.08.011

Jin Y, Chang J, Shi Y, Shi L, Hong S, Wang P (2018) A highly flexible and washable nonwoven photothermal cloth for efficient and practical solar steam generation. J Mater Chem A 6:7942–7949. https://doi.org/10.1039/C8TA00187A

Jones N, Ray B, Ranjit KT, Manna AC (2008) Antibacterial activity of ZnO nanoparticle suspensions on a broad spectrum of microorganisms. FEMS Microbiol Lett 279:71–76

Jung YH, Chang T-H, Zhang H, Yao C, Zheng Q, Yang VW, Mi H, Kim M, Cho SJ, Park D-W, Jiang H, Lee J, Qiu Y, Zhou W, Cai Z, Gong S, Ma Z (2015) High-performance green flexible electronics based on biodegradable cellulose nanofibril paper. Nat Commun 6:7170. https://doi.org/10.1038/ncomms8170

Karimi-Nazarabad M, Goharshadi EK, Mehrkhah R, Davardoostmanesh M (2021) Highly efficient clean water production: Reduced graphene oxide/ graphitic carbon nitride/wood. Sep Purif Technol. https://doi.org/10.1016/j.seppur.2021.119788

Kashyap V, Ghasemi H (2020) Solar heat localization: concept and emerging applications. J Mater Chem A 8:7035–7065. https://doi.org/10.1039/d0ta01004a

Kaur M, Ishii S, Shinde SL, Nagao T (2019) All-ceramic solar-driven water purifier based on anodized aluminum oxide and plasmonic titanium nitride. Adv Sustain Syst 3:1800112

Kim K, Yu S, An C, Kim S-W, Jang J-H (2018) Mesoporous Three-dimensional graphene networks for highly efficient solar desalination under 1 sun illumination. ACS Appl Mater Interfaces 10:15602–15608. https://doi.org/10.1021/acsami.7b19584

Kim K, Kang J, Kim SI, Kim S, Ryu ST, Jang JH (2020a) Recycling of particulate photoabsorbers for highly stable solar desalination operation. ACS Appl Energy Mater 3:8295–8301. https://doi.org/10.1021/acsaem.0c00824

Kim S, Kim K, Jun G, Hwang W (2020b) Wood-nanotechnology-based membrane for the efficient purification of oil-in-water emulsions. ACS Nano 14:17233–17240. https://doi.org/10.1021/acsnano.0c07206

Kiriarachchi HD, Awad FS, Hassan AA, Bobb JA, Lin A, El-Shall MS (2018) Plasmonic chemically modified cotton nanocomposite fibers for efficient solar water desalination and wastewater treatment. Nanoscale 10:18531–18539. https://doi.org/10.1039/C8NR05916K

Kou H, Liu Z, Zhu B, Macharia DK, Ahmed S, Wu B, Zhu M, Liu X, Chen Z (2019) Recyclable CNT-coupled cotton fabrics for low-cost and efficient desalination of seawater under sunlight. Desalination 462:29–38. https://doi.org/10.1016/j.desal.2019.04.005

Kuang Y, Chen C, Chen G, Pei Y, Pastel G, Jia C, Song J, Mi R, Yang B, Das S, Hu L (2019a) Bioinspired solar-heated carbon absorbent for efficient cleanup of highly viscous crude oil. Adv Funct Mater 29:1900162. https://doi.org/10.1002/adfm.201900162

Kuang Y, Chen C, He S, Hitz EM, Wang Y, Gan W, Mi R, Hu L (2019b) A high-performance self-regenerating solar evaporator for continuous water desalination. Adv Mater 31:1–8. https://doi.org/10.1002/adma.201900498

Kumar L, Ragunathan V, Chugh M, Bharadvaja N (2021) Nanomaterials for remediation of contaminants: a review. Environ Chem Lett 19:3139–3163. https://doi.org/10.1007/s10311-021-01212-z

Lee J, Kim K, Park SH, Yoon GY, Kim J, Lee SJ (2020) Macroporous photothermal bilayer evaporator for highly efficient and self-cleaning solar desalination. Nano Energy 77:105130. https://doi.org/10.1016/j.nanoen.2020.105130

Lei W, Ren K, Chen T, Chen X, Li B, Chang H, Ji J (2016) Polydopamine nanocoating for effective photothermal killing of bacteria and fungus upon near-infrared irradiation. Adv Mater Interfaces 3:1600767. https://doi.org/10.1002/admi.201600767

Lei Y, Xie L, Cao S, Wang Z, Du H, Sun K, Wang D, Zhang Y (2021) Application of wooden arrays in solar water evaporation and desalination. Mater Today Commun 29:102819. https://doi.org/10.1016/j.mtcomm.2021.102819

Li T, Zhu M, Yang Z, Song J, Dai J, Yao Y, Luo W, Pastel G, Yang B, Hu L (2016a) Wood composite as an energy efficient building material: guided sunlight transmittance and effective thermal insulation. Adv Energy Mater 6:1601122. https://doi.org/10.1002/aenm.201601122

Li X, Xu W, Tang M, Zhou L, Zhu B, Zhu S, Zhu J (2016b) Graphene oxide-based efficient and scalable solar desalination

under one sun with a confined 2D water path. Proc Natl Acad Sci 113:13953–13958. https://doi.org/10.1073/pnas.1613031113
Li Y, Gao T, Yang Z, Chen C, Kuang Y, Song J, Jia C, Hitz EM, Yang B, Hu L (2017a) Graphene oxide-based evaporator with one-dimensional water transport enabling high-efficiency solar desalination. Nano Energy 41:201–209
Li Y, Gao T, Yang Z, Chen C, Luo W, Song J, Hitz E, Jia C, Zhou Y, Liu B, Yang B, Hu L (2017b) 3D-printed, all-in-one evaporator for high-efficiency solar steam generation under 1 sun illumination. Adv Mater 29:1700981. https://doi.org/10.1002/adma.201700981
Li G, Law WC, Chan KC (2018a) Floating, highly efficient, and scalable graphene membranes for seawater desalination using solar energy. Green Chem 20:3689–3695. https://doi.org/10.1039/c8gc01347k
Li T, Liu H, Zhao X, Chen G, Dai J, Pastel G, Jia C, Chen C, Hitz E, Siddhartha D, Yang R, Hu L (2018b) Scalable and highly efficient mesoporous wood-based solar steam generation device: localized heat, rapid water transport. Adv Funct Mater 28:1–8. https://doi.org/10.1002/adfm.201707134
Li X, Li J, Lu J, Xu N, Chen C, Min X, Zhu B, Li H, Zhou L, Zhu S, Zhang T, Zhu J (2018c) Enhancement of interfacial solar vapor generation by environmental energy. Joule 2:1331–1338. https://doi.org/10.1016/j.joule.2018.04.004
Li X, Lin R, Ni G, Xu N, Hu X, Zhu B, Lv G, Li J, Zhu S, Zhu J (2018d) Three-dimensional artificial transpiration for efficient solar waste-water treatment. Natl Sci Rev 5:70–77. https://doi.org/10.1093/nsr/nwx051
Li C, Jiang D, Huo B, Ding M, Huang C, Jia D, Li H, Liu C-Y, Liu J (2019a) Scalable and robust bilayer polymer foams for highly efficient and stable solar desalination. Nano Energy 60:841–849
Li F, Li L, Zhong G, Zhai Y, Li Z (2019b) Effects of ultrasonic time, size of aggregates and temperature on the stability and viscosity of Cu-ethylene glycol (EG) nanofluids. Int J Heat Mass Transf 129:278–286. https://doi.org/10.1016/j.ijheatmasstransfer.2018.09.104
Li Z, Wang C, Lei T, Ma H, Su J, Ling S, Wang W (2019c) Arched bamboo charcoal as interfacial solar steam generation integrative device with enhanced water purification capacity. Adv Sustain Syst 3:1800144. https://doi.org/10.1002/adsu.201800144
Li Z, Zheng M, Wei N, Lin Y, Chu W, Xu R, Wang H, Tian J, Cui H (2020) Broadband-absorbing WO3-x nanorod-decorated wood evaporator for highly efficient solar-driven interfacial steam generation. Sol Energy Mater Sol Cells 205:110254. https://doi.org/10.1016/j.solmat.2019.110254
Li C, Yang J, Zhang L, Li S, Yuan Y, Xiao X, Fan X, Song C (2021a) Carbon-based membrane materials and applications in water and wastewater treatment: a review. Environ Chem Lett 19:1457–1475. https://doi.org/10.1007/s10311-020-01112-8
Li D, Han D, Guo C, Huang C (2021b) Facile preparation of MnO2-deposited wood for high-efficiency solar steam generation. ACS Appl Energy Mater 4:1752–1762. https://doi.org/10.1021/acsaem.0c02902
Li W, Li X, Liu J, Zeng M, Feng X, Jia X, Yu Z-Z (2021c) Coating of wood with Fe2O3-decorated carbon nanotubes by one-step combustion for efficient solar steam generation. ACS Appl Mater Interfaces 13:22845–22854. https://doi.org/10.1021/acsami.1c03388
Li Z, Cai W, Wang X, Hu Y, Gui Z (2021d) Self-floating black phosphorous nanosheets as a carry-on solar vapor generator. J Colloid Interface Sci 582:496–505. https://doi.org/10.1016/j.jcis.2020.08.073
Lin Y, Xu H, Shan X, Di Y, Zhao A, Hu Y, Gan Z (2019) Solar steam generation based on the photothermal effect: from designs to applications, and beyond. J Mater Chem A 7:19203–19227. https://doi.org/10.1039/c9ta05935k
Liu X, Xuan Y (2017) Full-spectrum volumetric solar thermal conversion: via photonic nanofluids. Nanoscale 9:14854–14860. https://doi.org/10.1039/c7nr03912c
Liu Y, Chen J, Guo D, Cao M, Jiang L (2015) Floatable, Self-cleaning, and carbon-black-based superhydrophobic gauze for the solar evaporation enhancement at the air-water interface. ACS Appl Mater Interfaces 7:13645–13652. https://doi.org/10.1021/acsami.5b03435
Liu C, Huang J, Hsiung C-E, Tian Y, Wang J, Han Y, Fratalocchi A (2017a) High-performance large-scale solar steam generation with nanolayers of reusable biomimetic nanoparticles. Adv Sustain Syst 1:1600013. https://doi.org/10.1002/adsu.201600013
Liu H, Zhang X, Hong Z, Pu Z, Yao Q, Shi J, Yang G, Mi B, Yang B, Liu X, Jiang H, Hu X (2017b) A bioinspired capillary-driven pump for solar vapor generation. Nano Energy 42:115–121. https://doi.org/10.1016/j.nanoen.2017.10.039
Liu K-K, Jiang Q, Tadepalli S, Raliya R, Biswas P, Naik RR, Singamaneni S (2017c) Wood-graphene oxide composite for highly efficient solar steam generation and desalination. ACS Appl Mater Interfaces 9:7675–7681. https://doi.org/10.1021/acsami.7b01307
Liu He, Chen C, Chen G, Kuang Y, Zhao X, Song J, Jia C, Xu X, Hitz E, Xie H, Wang S, Jiang F, Li T, Li Y, Gong A, Yang R, Das S, Hu L (2018a) High-performance solar steam device with layered channels: artificial tree with a reversed design. Adv Energy Mater 8:1701616. https://doi.org/10.1002/aenm.201701616
Liu H, Chen C, Wen H, Guo R, Williams NA, Wang B, Chen F, Hu L (2018b) Narrow bandgap semiconductor decorated wood membrane for high-efficiency solar-assisted water purification. J Mater Chem A 6:18839–18846. https://doi.org/10.1039/C8TA05924A
Liu PF, Miao L, Deng Z, Zhou J, Su H, Sun L, Tanemura S, Cao W, Jiang F, Zhao LD (2018c) A mimetic transpiration system for record high conversion efficiency in solar steam generator under one-sun. Mater Today Energy 8:166–173. https://doi.org/10.1016/j.mtener.2018.04.004
Liu X, Wang X, Huang J, Cheng G, He Y (2018d) Volumetric solar steam generation enhanced by reduced graphene oxide nanofluid. Appl Energy 220:302–312. https://doi.org/10.1016/j.apenergy.2018.03.097
Liu J, Liu Q, Ma D, Yuan Y, Yao J, Zhang W, Su H, Su Y, Gu J, Zhang D (2019a) Simultaneously achieving thermal insulation and rapid water transport in sugarcane stems for efficient solar steam generation. J Mater Chem A 7:9034–9039. https://doi.org/10.1039/c9ta00843h
Liu P-F, Miao L, Deng Z, Zhou J, Gu Y, Chen S, Cai H, Sun L, Tanemura S (2019b) Flame-treated and fast-assembled foam system for direct solar steam generation and non-plugging high salinity desalination with self-cleaning effect. Appl Energy 241:652–659
Liu S, Huang C, Luo X, Guo C (2019c) Performance optimization of bi-layer solar steam generation system through tuning porosity of bottom layer. Appl Energy 239:504–513. https://doi.org/10.1016/j.apenergy.2019.01.254
Liu H, Liu Y, Wang L, Qin X, Yu J (2021) Nanofiber based origami evaporator for multifunctional and omnidirectional solar steam generation. Carbonny 177:199–206
Lopes JL, Martins MJ, Nogueira HIS, Estrada AC, Trindade T (2021) Carbon-based heterogeneous photocatalysts for water cleaning technologies: a review. Environ Chem Lett 19:643–668. https://doi.org/10.1007/s10311-020-01092-9
Luo X, Ma C, Chen Z, Zhang X, Niu N, Li J, Liu S, Li S (2019) Biomass-derived solar-to-thermal materials: promising energy absorbers to convert light to mechanical motion. J Mater Chem A 7:4002–4008. https://doi.org/10.1039/C8TA11199E

Luo YQ, Song F, Wu JM, Wang F, Wang XL, Wang YZ (2021a) A nature-inspired suspended solar evaporator for water desalination of high-salinity brines. Chem Eng J 421:129824. https://doi.org/10.1016/j.cej.2021.129824

Luo ZY, Wang D, Chen KX, Huang L, Liu X, Zhang Q, Zhu H, Zhu S (2021b) Metal oxy-hydroxides with a hierarchical and hollow structure for highly efficient solar-thermal water evaporation. ACS Appl Mater Interfaces 13:27726–27733. https://doi.org/10.1021/acsami.1c09398

Ma N, Fu Q, Hong Y, Hao X, Wang X, Ju J, Sun J (2020) Processing natural wood into an efficient and durable solar steam generation device. ACS Appl Mater Interfaces 12:18165–18173. https://doi.org/10.1021/acsami.0c02481

Mahian O, Kolsi L, Amani M, Estellé P, Ahmadi G, Kleinstreuer C, Marshall JS, Siavashi M, Taylor RA, Niazmand H, Wongwises S, Hayat T, Kolanjiyil A, Kasaeian A, Pop I (2019) Recent advances in modeling and simulation of nanofluid flows-Part I: fundamentals and theory. Phys Rep 790:1–48. https://doi.org/10.1016/j.physrep.2018.11.004

Mehrkhah R, Goharshadi EK, Mohammadi M (2021a) Highly efficient solar desalination and wastewater treatment by economical wood-based double-layer photoabsorbers. J Ind Eng Chem 101:334–347

Mehrkhah R, Goharshadi EK, Mustafa M (2021b) Clean water production by non-noble metal / reduced graphene oxide nanocomposite coated on wood : scalable interfacial solar steam generation and heavy metal sorption. Sol Energy 224:440–454. https://doi.org/10.1016/j.solener.2021.06.004

Mehrkhah R, Ghafurian MM, Niazmand H, Goharshadi EK, Mahian O (2022) The use of nanofluids in solar desalination of saline water resources as antibacterial agents. In: Ali, H.M.B.T.-A. In: N.H.T. (Ed.), Advances in Nanofluid Heat Transfer. Elsevier, pp 265–301. https://doi.org/10.1016/B978-0-323-88656-7.00009-X

Mekonnen MM, Hoekstra AY (2016) Sustainability: four billion people facing severe water scarcity. Sci Adv 2:1–7. https://doi.org/10.1126/sciadv.1500323

Meng T, Jiang B, Li Z, Xu X, Li D, Henzie J, Nanjundan AK, Yamauchi Y, Bando Y (2021) Programmed design of selectively-functionalized wood aerogel: affordable and mildew-resistant solar-driven evaporator. Nano Energy 87:106146. https://doi.org/10.1016/j.nanoen.2021.106146

Moghayedi M, Goharshadi EK, Ghazvini K, Ahmadzadeh H, Ludwig R, Namayandeh-Jorabchi M (2017a) Improving antibacterial activity of phosphomolybdic acid using graphene. Mater Chem Phys 188:58–67

Moghayedi M, Goharshadi EK, Ghazvini K, Ahmadzadeh H, Ranjbaran L, Masoudi R, Ludwig R (2017b) Kinetics and mechanism of antibacterial activity and cytotoxicity of Ag-RGO nanocomposite. Colloids Surfaces B Biointerfaces 159:366–374

Moghayedi M, Goharshadi EK, Ghazvini K, Ahmadzadeh H, Jorabchi MN (2020) Antibacterial activity of Ag nanoparticles/phosphomolybdate/reduced graphene oxide nanocomposite: kinetics and mechanism insights. Mater Sci Eng B 262:114709

Morciano M, Fasano M, Salomov U, Ventola L, Chiavazzo E, Asinari P (2017) Efficient steam generation by inexpensive narrow gap evaporation device for solar applications. Sci Rep 7:1–9. https://doi.org/10.1038/s41598-017-12152-6

Mu X, Gu Y, Wang P, Wei A, Tian Y, Zhou J, Chen Y, Zhang J, Sun Z, Liu J, Sun L, Tanemura S (2021) Solar energy materials and solar cells strategies for breaking theoretical evaporation limitation in direct solar steam generation. Sol Energy Mater Sol Cells 220:110842. https://doi.org/10.1016/j.solmat.2020.110842

Ni G, Li G, Boriskina SV, Li H, Yang W, Zhang TJ, Chen G (2016) Steam generation under one sun enabled by a floating structure with thermal concentration. Nat Energy 1:1–7. https://doi.org/10.1038/nenergy.2016.126

Ni G, Zandavi SH, Javid SM, Boriskina SV, Cooper TA, Chen G (2018) A salt-rejecting floating solar still for low-cost desalination. Energy Environ Sci 11:1510–1519. https://doi.org/10.1039/c8ee00220g

Noureen L, Xie Z, Hussain M, Li M, Lyu Q, Wang K, Zhang L, Zhu J (2021) BiVO4 and reduced graphene oxide composite hydrogels for solar-driven steam generation and decontamination of polluted water. Sol Energy Mater Sol Cells 222:110952

Peng H, Guo J (2020) Removal of chromium from wastewater by membrane filtration, chemical precipitation, ion exchange, adsorption electrocoagulation, electrochemical reduction, electrodialysis, electrodeionization, photocatalysis and nanotechnology: a review. Environ Chem Lett 18:2055–2068. https://doi.org/10.1007/s10311-020-01058-x

Peng F, Xu J, Bai X, Feng G, Zeng X, Ibn Raihan MR, Bao H (2021) A janus solar evaporator with 2D water path for highly efficient salt-resisting solar steam generation. Sol Energy Mater Sol Cells 221:110910. https://doi.org/10.1016/j.solmat.2020.110910

Pilch-wr A, Marciniak Ł, Schuck PJ, Bednarkiewicz A, (2021) Standardization of methodology of light-to-heat conversion efficiency determination for colloidal nanoheaters.

Qin Z, Sun H, Tang Y, Yin S, Yang L, Xu M, Liu Z (2021) Bioinspired Hydrophilic-Hydrophobic Janus Composites for Highly Efficient Solar Steam Generation. ACS Appl Mater Interfaces 13:19467–19475

Qiu P, Liu F, Xu C, Chen H, Jiang F, Li Y, Guo Z (2019) Porous three-dimensional carbon foams with interconnected microchannels for high-efficiency solar-to-vapor conversion and desalination. J Mater Chem A 7:13036–13042. https://doi.org/10.1039/C9TA00041K

Ramanathan AA, Aqra MW, Al-Rawajfeh AE (2018) Recent advances in 2D nanopores for desalination. Environ Chem Lett 16:1217–1231. https://doi.org/10.1007/s10311-018-0745-4

Ren H, Tang M, Guan B, Wang K, Yang J, Wang F, Wang M, Shan J, Chen Z, Wei D, Peng H, Liu Z (2017) Hierarchical graphene foam for efficient omnidirectional solar-thermal energy conversion. Adv Mater 29:1702590. https://doi.org/10.1002/adma.201702590

Ren J, Liu Q, Pei Y, Wang Y, Yang S, Lin S, Chen W, Ling S, Kaplan DL (2021) Bioinspired energy storage and harvesting devices. Adv Mater Technol 6:1–16. https://doi.org/10.1002/admt.202001301

Rohrbach K, Li Y, Zhu H, Liu Z, Dai J, Andreasen J, Hu L (2014) A cellulose based hydrophilic, oleophobic hydrated filter for water/oil separation. Chem Commun 50:13296–13299

Rufus A, Sreeju N, Philip D (2016) Synthesis of biogenic hematite (α-Fe2O3) nanoparticles for antibacterial and nanofluid applications. RSC Adv 6:94206–94217. https://doi.org/10.1039/c6ra20240c

Sharma SK, Gupta SM (2016) Preparation and evaluation of stable nanofluids for heat transfer application: a review. Exp Therm Fluid Sci 79:202–212. https://doi.org/10.1016/j.expthermflusci.2016.06.029

Sheikhpour M, Arabi M, Kasaeian A, Rabei AR, Taherian Z (2020) Role of nanofluids in drug delivery and biomedical technology: Methods and applications. Nanotechnol Sci Appl 13:47–59. https://doi.org/10.2147/NSA.S260374

Sheng C, Yang N, Yan Y, Shen X, Jin C, Wang Z, Sun Q (2020) Bamboo decorated with plasmonic nanoparticles for efficient solar steam generation. Appl Therm Eng 167:114712. https://doi.org/10.1016/j.applthermaleng.2019.114712

Shi Y, Li R, Jin Y, Zhuo S, Shi L, Chang J, Hong S, Ng KC, Wang P (2018) A 3D Photothermal structure toward improved energy

efficiency in solar steam generation. Joule 2:1171–1186. https://doi.org/10.1016/j.joule.2018.03.013
Slavin YN, Asnis J, Häfeli UO, Bach H (2017) Metal nanoparticles: understanding the mechanisms behind antibacterial activity. J Nanobiotechnology 15:65. https://doi.org/10.1186/s12951-017-0308-z
Soares SF, Fernandes T, Trindade T, Daniel-da-Silva AL (2020) Recent advances on magnetic biosorbents and their applications for water treatment. Environ Chem Lett 18:151–164. https://doi.org/10.1007/s10311-019-00931-8
Song C, Li T, Guo W, Gao Y, Yang C, Zhang Q, An D, Huang W, Yan M, Guo C (2018) Hydrophobic Cu12Sb4S13-deposited photothermal film for interfacial water evaporation and thermal antibacterial activity. New J Chem 42:3175–3179. https://doi.org/10.1039/c7nj04545j
Song P, Cui J, Di J, Liu D, Xu M, Tang B, Zeng Q, Xiong J, Wang C, He Q (2019) Carbon microtube aerogel derived from kapok fiber: an efficient and recyclable sorbent for oils and organic solvents. ACS Nano 14:595–602
Song L, Zhang XF, Wang Z, Zheng T, Yao J (2021) Fe3O4/polyvinyl alcohol decorated delignified wood evaporator for continuous solar steam generation. Desalination 507:115024. https://doi.org/10.1016/j.desal.2021.115024
Struchalin PG, Ulset ET, Kosinski P, Zh S, He Y, Balakin BV (2021) Comparative analysis of photothermal boiling of water enhanced by nano- and micro-particles of carbon black. Mater Lett 285:129078. https://doi.org/10.1016/j.matlet.2020.129078
Sun F, Liu W, Dong Z, Deng Y (2017) Underwater superoleophobicity cellulose nanofibril aerogel through regioselective sulfonation for oil/water separation. Chem Eng J 330:774–782
Sun P, Zhang W, Zada I, Zhang Y, Gu J, Liu Q, Su H, Pantelić D, Jelenković B, Zhang D (2020a) 3D-structured carbonized sunflower heads for improved energy efficiency in solar steam generation. ACS Appl Mater Interfaces 12:2171–2179. https://doi.org/10.1021/acsami.9b11738
Sun Z, Li W, Song W, Zhang L, Wang Z (2020b) A high-efficiency solar desalination evaporator composite of corn stalk, Mcnts and TiO2: ultra-fast capillary water moisture transportation and porous bio-tissue multi-layer filtration. J Mater Chem A 8:349–357. https://doi.org/10.1039/c9ta10898j
Tao P, Ni G, Song C, Shang W, Wu J, Zhu J, Chen G, Deng T (2018) Solar-driven interfacial evaporation. Nat Energy 3:1031–1041. https://doi.org/10.1038/s41560-018-0260-7
Tao F, Green M, Garcia AV, Xiao T, Van Tran AT, Zhang Y, Yin Y, Chen X (2019) Recent progress of nanostructured interfacial solar vapor generators. Appl Mater Today 17:45–84. https://doi.org/10.1016/j.apmt.2019.07.011
Tian C, Liu J, Ruan R, Tian X, Lai X, Xing L, Su Y, Huang W, Cao Y, Tu J (2020) Sandwich photothermal membrane with confined hierarchical carbon cells enabling high-efficiency solar steam generation. Small 16:1–10. https://doi.org/10.1002/smll.202000573
Vay O, De Borst K, Hansmann C, Teischinger A, Müller U (2015) Thermal conductivity of wood at angles to the principal anatomical directions. Wood Sci Technol 49:577–589. https://doi.org/10.1007/s00226-015-0716-x
Villaseñor MJ, Ríos Á (2018) Nanomaterials for water cleaning and desalination, energy production, disinfection, agriculture and green chemistry. Environ Chem Lett 16:11–34. https://doi.org/10.1007/s10311-017-0656-9
Wang G, He Y, Wang H, Zhang L, Yu Q, Peng S, Wu X, Ren T, Zeng Z, Xue Q (2015) A cellulose sponge with robust superhydrophilicity and under-water superoleophobicity for highly effective oil/water separation. Green Chem 17:3093–3099
Wang X, He Y, Cheng G, Shi L, Liu X, Zhu J (2016a) Direct vapor generation through localized solar heating via carbon-nanotube nanofluid. Energy Convers Manag 130:176–183. https://doi.org/10.1016/j.enconman.2016.10.049
Wang Y, Zhang L, Wang P (2016b) Self-floating carbon nanotube membrane on macroporous silica substrate for highly efficient solar-driven interfacial water evaporation. ACS Sustain Chem Eng 4:1223–1230. https://doi.org/10.1021/acssuschemeng.5b01274
Wang J, Li Y, Deng L, Wei N, Weng Y, Dong S, Qi D, Qiu J, Chen X, Wu T (2017a) High-performance photothermal conversion of narrow-bandgap Ti2O3 nanoparticles. Adv Mater 29:1603730. https://doi.org/10.1002/adma.201603730
Wang J, Li Y, Deng L, Wei N, Weng Y, Dong S, Qi D, Qiu J, Chen X, Wu T (2017b) High-performance photothermal conversion of narrow-bandgap Ti2O3 nanoparticles. Adv Mater 29:1–6. https://doi.org/10.1002/adma.201603730
Wang X, He Y, Liu X, Cheng G, Zhu J (2017c) Solar steam generation through bio-inspired interface heating of broadband-absorbing plasmonic membranes. Appl Energy 195:414–425. https://doi.org/10.1016/j.apenergy.2017.03.080
Wang K, Liu X, Tan Y, Zhang W, Zhang S, Li J (2019a) Two-dimensional membrane and three-dimensional bulk aerogel materials via top-down wood nanotechnology for multibehavioral and reusable oil/water separation. Chem Eng J 371:769–780
Wang X, Liu Q, Wu S, Xu B, Xu H (2019b) Multilayer polypyrrole nanosheets with self-organized surface structures for flexible and efficient solar-thermal energy conversion. Adv Mater 31:1–9. https://doi.org/10.1002/adma.201807716
Wang Z, Yan Y, Shen X, Sun Q, Jin C (2019c) Candle soot nanoparticle-decorated wood for efficient solar vapor generation. Sustain Energy Fuels 4:354–361. https://doi.org/10.1039/c9se00617f
Wang K, Cheng Z, Li P, Zheng Y, Liu Z, Cui L, Xu J, Liu J (2021a) Three-dimensional self-floating foam composite impregnated with porous carbon and polyaniline for solar steam generation. J Colloid Interface Sci 581:504–513. https://doi.org/10.1016/j.jcis.2020.07.136
Wang M, Sun T, Wan D, Dai M, Ling S, Wang J, Liu Y, Fang Y, Xu S, Yeo J (2021b) Solar-powered nanostructured biopolymer hygroscopic aerogels for atmospheric water harvesting. Nano Energy 80:105569
Wang Q, Qin Y, Jia F, Li Y, Song S (2021c) Magnetic MoS2 nanosheets as recyclable solar-absorbers for high-performance solar steam generation. Renew Energy 163:146–153. https://doi.org/10.1016/j.renene.2020.07.019
Wang Y, Qi Q, Fan J, Wang W, Yu D (2021d) Simple and robust MXene/carbon nanotubes/cotton fabrics for textile wastewater purification via solar-driven interfacial water evaporation. Sep Purif Technol 254:117615. https://doi.org/10.1016/j.seppur.2020.117615
Wang Z, Wu X, Dong J, Yang X, He F, Peng S, Li Y (2022a) Porifera-inspired cost-effective and scalable "porous hydrogel sponge" for durable and highly efficient solar-driven desalination. Chem Eng J 427:130905
Wang Z, Wu X, Dong J, Yang X, He F, Peng S, Li Y (2022b) Porifera-inspired cost-effective and scalable "porous hydrogel sponge" for durable and highly efficient solar-driven desalination. Chem Eng J. https://doi.org/10.1016/j.cej.2021.130905
Wei A, Cui K, Wang P, Gu Y, Wang X, Mu X, Tian Y, Zhou J, Sun Z, Chen Y (2021) Multifunctional hydrothermal-carbonized sugarcane for highly efficient direct solar steam generation. Sol RRL 5:2000782
Wilson HM, Ahirrao DJ, Raheman Ar S, Jha N (2020) Biomass-derived porous carbon for excellent low intensity solar steam

generation and seawater desalination. Sol Energy Mater Sol Cells 215:110604. https://doi.org/10.1016/j.solmat.2020.110604
Wu X, Chen GY, Zhang W, Liu X, Xu H (2017) A plant-transpiration-process-inspired strategy for highly efficient solar evaporation. Adv Sustain Syst 1:1700046. https://doi.org/10.1002/adsu.201700046
Wu D, Qu D, Jiang W, Chen G, An L, Zhuang C, Sun Z (2019a) Self-floating nanostructured Ni–NiOx/Ni foam for solar thermal water evaporation. J Mater Chem A 7:8485–8490. https://doi.org/10.1039/C9TA00529C
Wu M-B, Hong Y-M, Liu C, Yang J, Wang X-P, Agarwal S, Greiner A, Xu Z-K (2019b) Delignified wood with unprecedented anti-oil properties for the highly efficient separation of crude oil/water mixtures. J Mater Chem A 7:16735–16741. https://doi.org/10.1039/C9TA04913D
Wu S, Xiong G, Yang H, Gong B, Tian Y, Xu C, Wang Y, Fisher T, Yan J, Cen K, Luo T, Tu X, Bo Z, Ostrikov K((2019c) Multifunctional solar waterways: plasma-enabled self-cleaning nanoarchitectures for energy-efficient desalination. Adv Energy Mater 9:1901286
Wu S-L, Chen H, Wang H-L, Chen X, Yang H-C, Darling SB (2021) Solar-driven evaporators for water treatment: challenges and opportunities. Environ Sci Water Res Technol 7:24–39
Xiao Y, Wang X, Li C, Peng H, Zhang T, Ye M (2021) A salt-rejecting solar evaporator for continuous steam generation. J Environ Chem Eng 9:105010
Xing C, Huang D, Chen S, Huang Q, Zhou C, Peng Z, Li J, Zhu X, Liu Y, Liu Z, Chen H (2019) Engineering lateral heterojunction of selenium-coated tellurium nanomaterials toward highly efficient solar. Desalination. https://doi.org/10.1002/advs.201900531
Xu X, Zhou J, Jiang L, Lubineau G, Ng T, Ooi BS, Liao H-Y, Shen C, Chen L, Zhu JY (2016) Highly transparent{,} low-haze{,} hybrid cellulose nanopaper as electrodes for flexible electronics. Nanoscale 8:12294–12306. https://doi.org/10.1039/C6NR02245F
Xu N, Hu X, Xu W, Li X, Zhou L, Zhu S, Zhu J (2017) Mushrooms as efficient solar steam-generation devices. Adv Mater 29:1606762
Xu W, Hu X, Zhuang S, Wang Y, Li X, Zhou L, Zhu S, Zhu J (2018) Flexible and salt resistant janus absorbers by electrospinning for stable and efficient solar desalination. Adv Energy Mater 8:1702884. https://doi.org/10.1002/aenm.201702884
Xu X, Long Y, Li Q, Li D, Mao D, Chen X, Chen Y (2019) Modified cellulose membrane with good durability for effective oil-in-water emulsion treatment. J Clean Prod 211:1463–1470
Xu Z, Zhang L, Zhao L, Li B, Bhatia B, Wang C, Wilke KL, Song Y, Labban O, Lienhard JH, Wang R, Wang EN (2020) Ultrahigh-efficiency desalination: via a thermally-localized multistage solar still. Energy Environ Sci 13:830–839. https://doi.org/10.1039/c9ee04122b
Xu R, Wei N, Li Z, Song X, Li Q, Sun K, Yang E, Gong L, Sui Y, Tian J, Wang X, Zhao M, Cui H (2021) Construction of hierarchical 2D/2D Ti3C2/MoS2 nanocomposites for high-efficiency solar steam generation. J Colloid Interface Sci 584:125–133. https://doi.org/10.1016/j.jcis.2020.09.052
Xue G, Liu K, Chen Q, Yang P, Li J, Ding T, Duan J, Qi B, Zhou J (2017) Robust and low-cost flame-treated wood for high-performance solar steam generation. ACS Appl Mater Int 9:15052–15057. https://doi.org/10.1021/acsami.7b01992
Yang X, Zheng ZC, Xu Y (2010) A study on flow through a periodic array of porous medium cylinders by immersed-boundary methods. In Fluids Eng Div Summer Meeting. https://doi.org/10.1115/FEDSM-ICNMM2010-30535
Yang Y, Zhao H, Yin Z, Zhao J, Yin X, Li N, Yin D, Li Y, Lei B, Du Y (2018a) A general salt-resistant hydrophilic/hydrophobic nanoporous double layer design for efficient and stable solar water evaporation distillation. Mater Horizons 5:1143–1150
Yang Y, Zhao R, Zhang T, Zhao K, Xiao P, Ma Y, Ajayan PM, Shi G, Chen Y (2018b) Graphene-based standalone solar energy converter for water desalination and purification. ACS Nano 12:829–835. https://doi.org/10.1021/acsnano.7b08196
Yang HC, Chen Z, Xie Y, Wang J, Elam JW, Li W, Darling SB (2019a) Chinese ink: a powerful photothermal material for solar steam generation. Adv Mater Int 6:1–7. https://doi.org/10.1002/admi.201801252
Yang Y, Que W, Zhao J, Han Y, Ju M, Yin X (2019b) Membrane assembled from anti-fouling copper-zinc-tin-selenide nanocarambolas for solar-driven interfacial water evaporation. Chem Eng J 373P:955–962
Yang J, Chen Y, Jia X, Li Y, Wang S, Song H (2020) Wood-based solar interface evaporation device with self-desalting and high antibacterial activity for efficient solar steam generation. ACS Appl Mater Interfaces 12:47029–47037. https://doi.org/10.1021/acsami.0c14068
Yin Z, Wang H, Jian M, Li Y, Xia K, Zhang M, Wang C, Wang Q, Ma M, Zheng Q (2017) Extremely black vertically aligned carbon nanotube arrays for solar steam generation. ACS Appl Mater Interfaces 9:28596–28603
Yu Z, Cheng S, Li C, Sun Y, Li B (2019) Enhancing efficiency of carbonized wood based solar steam generator for wastewater treatment by optimizing the thickness. Sol Energy 193:434–441. https://doi.org/10.1016/j.solener.2019.09.080
Yuan B, Li L, Murugadoss V, Vupputuri S, Wang J, Alikhani N, Guo Z (2020) Nanocellulose-based composite materials for wastewater treatment and waste-oil remediation. ES Food Agrofor. https://doi.org/10.30919/esfaf0004
Yue X, Li J, Zhang T, Qiu F, Yang D, Xue M (2017) In situ one-step fabrication of durable superhydrophobic-superoleophilic cellulose/LDH membrane with hierarchical structure for efficiency oil/water separation. Chem Eng J 328:117–123
Zareei M, Yoozbashizadeh H, Madaah Hosseini HR (2019) Investigating the effects of pH, surfactant and ionic strength on the stability of alumina/water nanofluids using DLVO theory. J Therm Anal Calorim 135:1185–1196. https://doi.org/10.1007/s10973-018-7620-1
Zehtabiyan-Rezaie N, Saffar-Avval M, Adamiak K (2021) Electrohydrodynamic water desalination: evaluating the productivity and energy consumption. Desalination 497:114768. https://doi.org/10.1016/j.desal.2020.114768
Zeiny A, Jin H, Bai L, Lin G, Wen D (2018) A comparative study of direct absorption nanofluids for solar thermal applications. Sol Energy 161:74–82. https://doi.org/10.1016/j.solener.2017.12.037
Zhang P, Li J, Lv L, Zhao Y, Qu L (2017) Vertically aligned graphene sheets membrane for highly efficient solar thermal generation of clean water. ACS Nano 11:5087–5093. https://doi.org/10.1021/acsnano.7b01965
Zhang P, Liao Q, Zhang T, Cheng H, Huang Y, Yang C, Li C, Jiang L, Qu L (2018a) High throughput of clean water excluding ions, organic media, and bacteria from defect-abundant graphene aerogel under sunlight. Nano Energy 46:415–422
Zhang Y, Ravi SK, Vaghasiya JV, Tan SC (2018b) A barbeque-analog route to carbonize moldy bread for efficient steam generation. Iscience 3:31–39
Zhang Y, Ravi SK, Tan SC (2019) Systematic study of the effects of system geometry and ambient conditions on solar steam generation for evaporation optimization. Adv Sustain Syst 3:1–7. https://doi.org/10.1002/adsu.201900044
Zhang Qi, Chen S, Fu Z, Yu H, Quan X (2020a) Temperature-difference-induced electricity during solar desalination with bilayer MXene-based monoliths. Nano Energy. https://doi.org/10.1016/j.nanoen.2020.105060
Zhang Q, Li L, Jiang B, Zhang H, He N, Yang S, Tang D, Song Y (2020b) Flexible and mildew-resistant wood-derived aerogel for

stable and efficient solar desalination. ACS Appl Mater Interfaces 12:28179–28187. https://doi.org/10.1021/acsami.0c05806

Zhang X, Yang L, Dang B, Tao J, Li S, Zhao S, Li W, Li J, Chen Z, Liu S (2020c) Nature-inspired design: p- toluenesulfonic acid-assisted hydrothermally engineered wood for solar steam generation. Nano Energy 78:105322. https://doi.org/10.1016/j.nanoen.2020.105322

Zhang C, Yuan B, Liang Y, Yang L, Bai L, Yang H, Wei D, Wang F, Wang Q, Wang W, Chen H (2021) Carbon nanofibers enhanced solar steam generation device based on loofah biomass for water purification. Mater Chem Phys 258:123998. https://doi.org/10.1016/j.matchemphys.2020.123998

Zhao F, Zhou X, Shi Y, Qian X, Alexander M, Zhao X, Mendez S, Yang R, Qu L, Yu G (2018a) Highly efficient solar vapour generation via hierarchically nanostructured gels. Nat Nanotechnol 13:489–495

Zhao J, Yang Y, Yang C, Tian Y, Han Y, Liu J, Yin X, Que W (2018c) A hydrophobic surface enabled salt-blocking 2D Ti3C2 MXene membrane for efficient and stable solar desalination. J Mater Chem A 6:16196–16204. https://doi.org/10.1039/C8TA05569F

Zhao X, Li Q, Li L, Hu T, Yang Y, Zhang J (2020) Facile preparation of polydimethylsiloxane/carbon nanotubes modified melamine solar evaporators for efficient steam generation and desalination. J Colloid Interface Sci. https://doi.org/10.1016/j.jcis.2020.10.002

Zhong J, Huang C, Wu D, Lin Z (2019) Influence factors of the evaporation rate of a solar steam generation system: A numerical study. Int J Heat Mass Transf 128:860–864

Zhou L, Tan Y, Ji D, Zhu B, Zhang P, Xu J, Gan Q, Yu Z, Zhu J (2016) Self-assembly of highly efficient, broadband plasmonic absorbers for solar steam generation. Sci Adv 2:e1501227. https://doi.org/10.1126/sciadv.1501227

Zhou X, Zhao F, Guo Y, Rosenberger B, Yu G (2019) Architecting highly hydratable polymer networks to tune the water state for solar water purification. Sci Adv. https://doi.org/10.1126/sciadv.aaw5484

Zhu G, Xu J, Zhao W, Huang F (2016a) Constructing black titania with unique nanocage structure for solar desalination. ACS Appl Mater Interfaces 8:31716–31721. https://doi.org/10.1021/acsami.6b11466

Zhu M, Li T, Davis CS, Yao Y, Dai J, Wang Y, AlQatari F, Gilman JW, Hu L (2016b) Transparent and haze wood composites for highly efficient broadband light management in solar cells. Nano Energy 26:332–339

Zhu M, Song J, Li T, Gong A, Wang Y, Dai J, Yao Y, Luo W, Henderson D, Hu L (2016c) Highly anisotropic, highly transparent wood composites. Adv Mater 28:5181–5187

Zhu M, Li Y, Chen G, Jiang F, Yang Z, Luo X, Wang Y, Lacey SD, Dai J, Wang C, Jia C, Wan J, Yao Y, Gong A, Yang B, Yu Z, Das S, Hu L (2017a) Tree-inspired design for high-efficiency water extraction. Adv Mater 29:1704107. https://doi.org/10.1002/adma.201704107

Zhu M, Wang Y, Zhu S, Xu L, Jia C, Dai J, Song J, Yao Y, Wang Y, Li Y, Henderson D, Luo W, Li H, Minus ML, Li T, Hu L (2017b) Anisotropic, transparent films with aligned cellulose nanofibers. Adv Mater 29:1606284. https://doi.org/10.1002/adma.201606284

Zhu L, Gao M, Kang C, Peh N, Wang X (2018a) Self-contained monolithic carbon sponges for solar-driven interfacial water evaporation distillation and electricity generation. Adv Energy Mater 1702149:1–8. https://doi.org/10.1002/aenm.201702149

Zhu M, Li Y, Chen F, Zhu X, Dai J, Li Y, Yang Z, Yan X, Song J, Wang Y, Hitz E, Luo W, Lu M, Yang B, Hu L (2018b) Plasmonic wood for high-efficiency solar steam generation. Adv Energy Mater 8:1–7. https://doi.org/10.1002/aenm.201701028

Zhu L, Ding T, Gao M, Kang C, Peh N, Ho GW (2019a) Shape conformal and thermal insulative organic solar absorber sponge for photothermal water evaporation and thermoelectric power generation. Adv Energy Mater 1900250:3–9. https://doi.org/10.1002/aenm.201900250

Zhu M, Yu J, Ma C, Zhang C, Wu D, Zhu H (2019b) Carbonized daikon for high efficient solar steam generation. Sol Energy Mater Sol Cells 191:83–90. https://doi.org/10.1016/j.solmat.2018.11.015

Zhu Z, Fu S, Lucia LA (2019c) A fiber-aligned thermal-managed wood-based superhydrophobic aerogel for efficient oil recovery. ACS Sustain Chem Eng 7:16428–16439. https://doi.org/10.1021/acssuschemeng.9b03544

Zielinski MS, Choi JW, La Grange T, Modestino M, Hashemi SMH, Pu Y, Birkhold S, Hubbell JA, Psaltis D (2016) Hollow mesoporous plasmonic nanoshells for enhanced solar vapor generation. Nano Lett 16:2159–2167. https://doi.org/10.1021/acs.nanolett.5b03901

Zou Y, Yang P, Yang L, Li N, Duan G, Liu X, Li Y (2021) Boosting solar steam generation by photothermal enhanced polydopamine/wood composites. Polymer (guildf) 217:123464

Zuo Y-M, Yan X, Xue J, Guo L-Y, Fang W-W, Sun T-C, Li M, Zha Z, Yu Q, Wang Y (2020) Enzyme-responsive Ag nanoparticle assemblies in targeting antibacterial against methicillin-resistant staphylococcus aureus. ACS Appl Mater Int 12:4333–4342